The Thesis Committee for Zhong Pan
Certifies that this is the approved version of the following thesis:

Revised Productivity Index Equation to Improve Transient History Match for the Capacitance Resistance Model

APPROVED BY
SUPERVISING COMMITTEE:

Supervisor:

Larry W. Lake

Kishore K. Mohanty

Revised Productivity Index Equation to Improve Transient History Match for the Capacitance Resistance Model

by

Zhong Pan, B.S.P.E

Thesis

Presented to the Faculty of the Graduate School of

The University of Texas at Austin

in Partial Fulfillment

of the Requirements

for the Degree of

Master of Science in Engineering

The University of Texas at Austin

December 2016

Dedication

To my parents Mingtai Pan and Yirong Yang for their endless love and support

To all the Spring Festivals that I have missed for the past six years

To the City of Austin for being my second home

Acknowledgements

I would like to express my sincere appreciation to my supervisor, friend, and mentor, Dr. Larry W. Lake for his continued encouragement and guidance. He has always been supportive of my decision both in and out of the office. It is an honor to be able to work with such a true scholar who is so intelligent and dedicated to the field of engineering. He will always be an exemplary figure that I look up to. His financial and most importantly moral support meant so much to me, and I can never get to where I am right now without him having my back. I deeply appreciate his help throughout these years.

I also want to thank Dr. Kishore K. Mohanty for being the second reader of this thesis and providing valuable comments. My appreciation goes to my colleagues, Brian Lee, Yun Wu, Bo Ren, and Behzad Eftekhari for all the laughter they brought to the office. They made my graduate study enjoyable. The Bakken field data from Hess is also deeply appreciated. Without their data, I can never accomplish this study.

Last but not least, I can never appreciate too much the abysmal trust and support from my parents. They always have firm believe in every decision I made and every path I decided to take. Without their support, I would not become what I am now, and would not be able to overcome all the obstacles during my six years in the US.

Abstract

Revised Productivity Index Equation to Improve Transient History Match for the Capacitance Resistance Model

Zhong Pan, M.S.E.

The University of Texas at Austin, 2016

Supervisor: Larry W. Lake

The Capacitance Resistance Model (CRM) is a data-driven reservoir model developed for well surveillance and management. The model is gaining popularity in reservoir engineering community because of its simplicity and ability to provide insights on well-to-well connectivity during water/gas flooding project. Furthermore, the model can be used to optimize injection scheme or even plan for infill drilling.

The model was built on the assumptions that during waterflooding the dominant flow regime is semi-steady state. However, to extend the functionality of this model to unconventional reservoirs, a productivity index model that works well in transient flow regime should be investigated.

In this thesis, two different productivity models are proposed. The first is the combined productivity index model. This model originates from the analytical solution of single compartment model and the constant behavior of the productivity index in fracture-dominated flow. These two components are then linearly combined to form a new productivity index model. The second is the logistic productivity index model, which

uses a well-studied logistic growth model to capture the S-shaped production profile starting from a transient linear flow regime to a late-time fracture-dominated regime. These two proposed productivity index models are incorporated into the fundamental CRM equation, respectively, to derive the logistic CRM and combined CRM.

To validate the models, multiple reservoir simulations were conducted to generate synthetic cases capturing both transient linear flow and fracture-dominated regime, and then the proposed models were fitted to the simulation data using Microsoft Excel Solver. Case validation is also accomplished with field data. Very good history matches were obtained from these two models, and they demonstrate that with proper revision to semi-steady state model CRM is able to match production history sufficiently and quickly. In addition, the combined CRM is physics-based so it is shown that the model is able to provide insights on some important reservoir properties.

Table of Contents

List of Tables

List of Figures

Chapter 1: Literature Review

CAPACITANCE RESISTANCE MODEL (CRM)

CRM is a computationally inexpensive reservoir model that combines a data-driven approach with reservoir physics to obtain a synergy between analytical and empirical models. CRM characterizes the connections among multiple injectors and producers and the response lag in an analogous way to the voltage across a capacitor in an RC circuit where the battery potential is equivalent to the injection signal.

In CRM, the material balance equation is established to calculate the contributions of the injection signals from each well and the injector to producer response time resulting from the fluid compressibility. The analogy of oil reservoir to a RC circuit is proposed by Bruce (1943) who is the first person to construct a physical electrical system that consisted of 2501 capacitors connected to 4900 resistors to simulate the performance of reservoirs in Saudi Arabia. The simulation device is able to match history pressure data really well in a data back test where only a portion of pressure data were used for the history match and the rest of the data were used to validate the forecast.

While the early work focused on experimental apparatus to simulate reservoir performance, Lake et al. (2002) used the same conceptual idea in a mathematical model. Albertoni and Lake (2003) suggested that the production response is a linearly-weighted combination of injection rates and that injection and production data only are sufficient to quantify the well communications. Yousef (2005) was the first to develop the mathematical model for CRM using the material balance equation. He proposed the concept of a time constant and well connectivity within CRM model. Additionally, he solved the CRM using discretization of time and extended the applicability of CRM to handle various BHP. He achieved synthetic and field cases validation with CRM, where he concluded that CRM model parameters can reasonably indicate reservoir geological

features (Yousef et al., 2006). Sayarpour (2008) obtained a semi-analytical solution of the governing differential equation of CRM with the superposition of time technique. He derived semi-analytical solutions with various reservoir control volumes, including single tank, producer-based drainage volume, and producer-injector drainage volume. He then incorporated the oil fractional flow theory into the model so that the predicted oil flow rate can be separated from the total liquid flow rate. His results were also validated with both synthetic and field cases. Weber (2009) switched to a more powerful optimizer GAMS to solve for the CRM parameters. The deployment of GAMS greatly extended CRM's capabilities to optimize field large data sets (Weber et al., 2009).

Cao (2014) advanced the mathematical model by solving both the pressure and saturation equations simultaneously. This enhanced model eliminates the assumption of single-phase flow and incorporates the two-phase displacement physics. Solving the saturation equation enabled saturation changes according to the reservoir dynamics, and thus the model can be applied to the entire history of water and gas flood rather than only the mature water floods, which is close to the single-phase flow. Because of the presence of the saturation equation, it is also convenient to calculate the oil saturation within the drainage volume of each producer as well as the average reservoir pressure for the entire field. Also, the oil fractional flow will be an output from solving the total and oil material balance equation, which facilitates more accurate oil rate prediction.

ANALYTICAL RESERVOIR MODEL FOR HYDRAULICALLY FRACTURED WELLS

Wattenbarger and El-Banbi (1998) presented a linear transient flow solution for hydraulically fractured wells under both constant pressure and constant rate boundary conditions. The mathematical model indicates that during the early time linear transient flow a log-log plot of production rate versus time shows a half-slope while the late time

solution for flow after pressure interference at the boundary interference shows an exponential decline. The Wattenbarger and El-Banbi solution was derived for slightly compressible liquid flow; however, the solution can be extended to gas flow if real gas pseudo-potential is used. Such solutions can be used to estimate $A\sqrt{k}$, reservoir drainage volume, and OOIP.

LOGISTIC GROWTH MODEL

Logistic growth models are a group of mathematical models formulated for various generic applications. They were originally developed for modeling population growth, and then extended to the natural science. The model was also used in analyzing the market penetration of new products (Tsoularis and Wallace, 2001) and even the oil production of entire regions (Hubbert, 1956).

Hubbert proposed a so-called Hubbert model to fit production profiles for various areas, and predicted the decline of US and North Sea oil production. Patzek (2010) proposed using multi-Hubert cycle analysis instead of single Hubbert curve to history match and forecast the production rate and cumulative production of gas in the Barnett Shale. Clark (2011), observing the similarity between a cumulative oil production history and population growth, used the logistic growth model to fit the decline of oil production over time. The model can fit the oil rate and cumulative production data from Bakken Shale really well.

Chapter 2: Simulation Validation of Single Compartment Model

The application of the CRM model is currently limited to pseudo-steady state flow regime. The reason is that the productivity index equation integrated into the material balance formulation only applies to pseudo-steady state. To extend the applicability of CRM, a productivity index equation for long period of transient regime is necessary.

Wattenbarger and El-Banbi (Wattenbarger and El-Banbi 1998) proposed a classic model to describe the fluid flow behavior in a fractured horizontal reservoir; the model is referred to as the single compartment model. This model assumes that the fluid flows through the formation matrix and enters directly into the wellbore, and the fracture is infinitely conductive so that it is just an extension of the wellbore. In contrast, the double compartment model assumes that the fluid flows through both formation matrix and the finitely conductive fracture to enter the wellbore. Only the single compartment model is relevant to the discussion in this work.

Figure 1 shows the geometry of the single compartment model and its control volume from which the later formulation is derived. In this section, multiple simulations were conducted to observe the transient behavior during the well production as in a single compartment model and serve as basis to formulate new productivity index equation to improve the performance of CRM for flow in unconventional reservoirs.

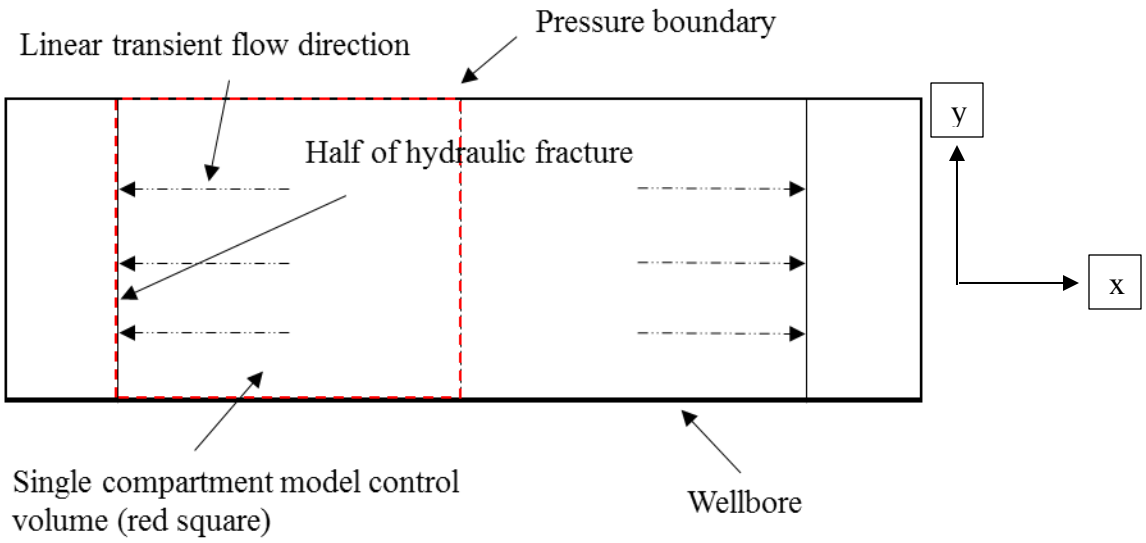

Figure 1: The reservoir and well geometry for single compartment model

SIMULATION DESCRIPTION

To examine the performance of fluid flow and the behavior of the productivity index in a single compartment model, a simplified spreadsheet simulation and both CMG IMEX model were used.

CMG IMEX Model

A 1D simulation by CMG IMEX was constructed according to the geometry described by Wattenbarger and El-Banbi (El-Banbi 1998). The reservoir model is 1400 ft and is divided into 300 grid blocks with 4 ft width for each grid block. The reservoir width is 200 ft, and the thickness is 10 ft. There is a vertical producer drilled at block (1, 1, 1). The parameter that differentiates the fracture and formation matrix is mainly permeability. The cell in which the well is located represents the fracture that has in theory infinitely large permeability, so in the simulation model the maximum permeability allowed by the simulator, 1E9 md, is assigned to that cell to represent the infinitely conductive fractures. All other cells have permeability much smaller than the

well cell, normally in the order of 0.01 to 1 md depending on the intended length of linear transient flow and semi-steady state respectively. The smaller the formation permeability, the longer the linear transient regime. The cell (300, 1, 1) represents the pressure boundary between two neighboring fractures. Under homogeneous reservoir assumption, when two neighboring fractures start producing, there will be pressure propagating simultaneously outward from both fractures, and the well starts to produce reservoir fluid under linear transient flow regime. The boundary-dominated flow regime begins when pressure waves from two sources start to interfere with each other. In a realistic homogeneous reservoir model, the pressure interference is assumed to happen half way between two nearby fractures, so in the simulation model cell (300, 1, 1) marks the pressure boundary.

The reservoir top is set to be 1000 ft below the ground, and the water-oil contact is set to be 1500 ft so that the initial oil saturation is 100%, eliminating the water production during the simulation. The bubble point is 5 psi, which set to be very small so that gas never bubbles out of the liquid. Throughout the simulation, the gas production under reservoir condition is always zero, which ensures that the simulator only simulates one phase fluid flow in the reservoir. All the fluid and reservoir parameters inputs in the reservoir simulation are in Table 1.

Many analytical solutions for reservoir flow regimes assume single-phase flow. In particular, such condition is assumed to derive the solutions for transient linear (Wattenbarger and El-Banbi1998) and semi-steady state regime (Walsh and Lake, 2003). The purpose of this thesis is to investigate the ways to improve the history match of CRM during linear transient flow regime. Simulation results in this case are the benchmark for later comparisons, so it is crucial to make sure that the simulation is built in such way that it meets all the requirement and assumptions of the analytical solutions. Furthermore, the

simulation results should include the characteristic behaviors of the particular flow regime, and then the model developed later can be compared to the base case. The simulator will automatically vary the time step to ensure the stability of the finite difference method for solving the differential equation implicitly, and the maximum time step sets the upper limit for the variations. By default, the maximum time step for simulation is 365 days. In the simulation model, a maximum time step was chosen to be either 2E-8 days or 365 days depending on the temporal resolution intended for the simulation. With the larger time step, it is easier to see the general trend. In comparison, if the maximum time step is set to be very small, many fluid flow details can be identified and analyzed. In this work, two different maximum time step sizes yield very different production history, and the difference will be discussed later.

The geometry of the reservoir simulation model is designed to replicate the geometry used to derive the analytical model, so the reservoir and well parameters are chosen to produce the typical production behavior. The numerical values for these parameters do not necessarily match up with the realistic production and geological conditions.

Parameter	Values
Number of cells	300
Cell dimensions, x×y×z	4×200×10
Porosity, %	0.21
Rock compressibility, 1/psi	3.7×10^{-5}
Oil Compressibility, 1/psi	1×10^{-7}
Reservoir temperature, F	168
Oil viscosity, cp	1
Water viscosity, cp	1
Fracture permeability, md	1×10^{9}
Matrix permeability, md	0.01-1
Bottom hole pressure, psi	10

Table 1: Selected reservoir simulation parameters

Spreadsheet Model

The spreadsheet simulator is a numerical simulator implemented in Excel using the fundamental reservoir simulation concepts to illustrate flow behavior in an undergraduate class. The simulator has 11 discretized blocks, each block of which was assigned a value for reservoir properties, including permeability, viscosity, oil compressibility, and porosity. The numerical model is capable of simulating non-uniform grid blocks; however, simulations with uniform grid block in all x, y, and z directions was investigated because of its simplicity for further analysis, so the block size in all three Cartesian coordinates were kept constant. The model is also able to simulate the one-dimensional flow in a radial flow coordinate system; however, the Cartesian Figure 2 shows the inputs in the spreadsheet model.

i=	1	2	3	4	5	6	7	8	9	10	11
delx, m=	20	20	20	20	20	20	20	20	20	20	20
dely, m=	50	50	50	50	50	50	50	50	50	50	50
delz, m	20	20	20	20	20	20	20	20	20	20	20
porosity, fr=	0.2	0.2	0.2	0.2	0.2	0.2	0.2	0.2	0.2	0.2	0.2
k, md=	5	5	5	5	5	5	5	5	5	5	5
viscosity, mPa-s	1	1	1	1	1	1	1	1	1	1	1
ct, GPa-1=	1	1	1	1	1	1	1	1	1	1	1

Figure 2: Parameter inputs in spreadsheet model

The pressure for each cell at each time step is calculated with the implicit method. Transmissibility measures how much fluid flows in or out of the grid block. For each grid block in the simulator, the transmissibility between a cell and its neighboring two cells can be written in a pressure equation. All pressure equations constitute an n-by-n matrix that then is inversed to calculate the cell pressures for the next time step simultaneously, as shown by the results in Figure 3.

i=	1	2	3	4	5	6	7	8	9	10	11
t,days	P, MPa										
	10.0	30.0	50.0	70.0	90.0	110.0	130.0	150.0	170.0	190.0	210.0
0	25.0	25.0	25.0	25.0	25.0	25.0	25.0	25.0	25.0	25.0	25.0
2.5	15.4	19.3	22.0	23.6	24.4	24.8	24.9	25.0	25.0	25.0	25.0
5	15.3	18.0	20.6	22.5	23.7	24.4	24.8	24.9	25.0	25.0	25.0
7.5	15.2	17.6	19.8	21.7	23.1	24.0	24.5	24.8	24.9	25.0	25.0
10	15.2	17.3	19.3	21.1	22.6	23.6	24.3	24.7	24.9	24.9	25.0

Figure 3: Pressure computation results from inverting matrix

After the pressure for each cell at every time step is calculated, the average reservoir pressure is then computed. The production rate for each time step is calculated with a simple well model represented as the productivity index, as shown in Equation 1.

$$q = J_{well}\left(P_{well\ cell} - P_{wf}\right) \quad (1)$$

In Equation 1, J characterizes the wellbore performance, and P_{wf} is the well bottom hole pressure. Well cell pressure is the result of inverting the pressure matrix as shown in Figure 4 above. After the average reservoir pressure is computed from all cell pressures, the productivity index for the simulated reservoir can be calculated by Equation 2.

$$J_{field} = \frac{q}{\left(\bar{P} - P_{wf}\right)} \quad (2)$$

FLUID FLOW CHARACTERISTICS OF SINGLE COMPARTMENT MODEL

CMG IMEX Simulations

Because of the numerical nature of the simulation, the choice of time step in the simulation has a huge impact on the flow performance and the behavior of its resulting production history. As shown in Figure 4, the production profile with maximum time step of 2×10^{-8} days declines dramatically from 10^9 bbl/day to 10000 in the first 1×10^{-6} days, and then the production hits a plateau period with constant production at 10000 bbl/day until 0.001 days. The curve resumes its linear decline on a log-log scale and then the curve enters a period of exponential decline. In comparison, the production

history with maximum time step of 1 day indicated on the plot in blue curve only possesses the last two sections.

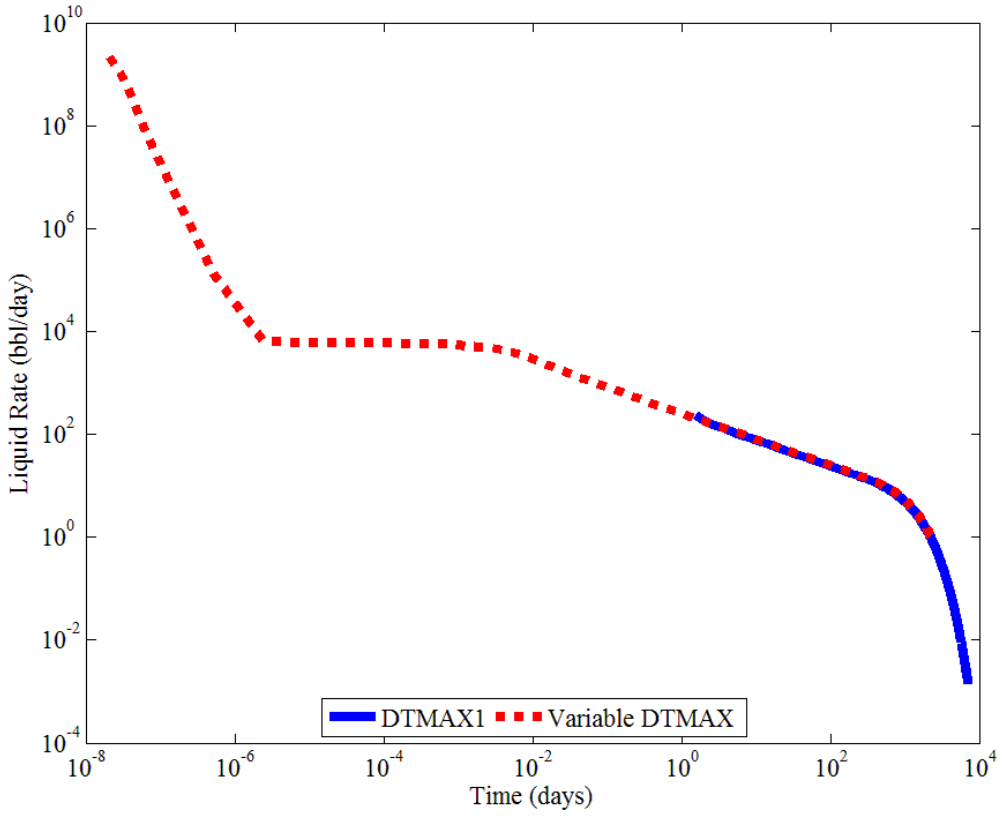

Figure 4: Production history for a single compartment model with two different maximum time steps

The differences between the two plots are because the permeability of the fracture block is huge yet still finite, which violates one of the important assumptions of the single compartment model. The ramification of this violation is that the pressure propagation in the first block is not instantaneous. As shown in a simulation result for a reservoir with permeability of 1 md in Figure 5, after the well is put on production, the well bottom hole pressure instantaneously drops to 10 psi, and since the permeability at the fracture block

is extremely large, though finite, the liquid starts to flow at a huge rate. As shown on the Pressure (1 1 1) curve, the cell pressure drops to 10 psi in 1E-6 days, which in theory should be 0 days. During this period, the pressure in cell (2, 1, 1) remains at the initial reservoir pressure. The fast reduction of cell pressure leads to a fast decline of liquid flow rate. This explanation is corroborated by the liquid rate ceasing to decline at the moment when the pressure at the fracture cell drops to 10 psi.

During the constant production period, the pressure at the fracture cell has already dropped to 10 psi, and the pressure in the next cell – according to the Pressure (2 1 1) curve – remains at the initial reservoir pressure. Such pressure differential is kept constant until 1E-3 days, which leads to a period of constant production. As the pressure drop is felt in the second cell, the production history enters a period of linear decline with one-half slope on a log-log scale, which is the transient flow from the reservoir matrix linearly to the fracture (El-Banbi and Wattenbarger, 1998).

The cell pressure at block (300, 1, 1) remains at the initial reservoir pressure while cells closer to the wellbore start to deviate from initial pressure at about 59 days when the farthest cell from the wellbore starts to deviate. The reservoir is assumed to be homogeneous, so the pressure propagation from the current and the neighboring fractures reach the middle point at the same time creating a no flow boundary to both fractures. When the pressure propagation reached the middle point, a transition is observed from linear decline on a log-log scale to a linear decline on a semi-log scale. This indicates the inception of the semi-steady state flow, a flow condition dominated by the impermeable flow boundary (Walsh and Lake, 2003).

In comparison, the simulation with maximum time step of 1 day shows only the linear transient flow regime and semi-steady state regime, since the resolution is not enough to capture the flow behavior resulted from the pressure depletion in the fracture

block. However, the geometry of the single compartment model excludes the observable pressure depletion in the fracture cell, so only the last two flow regimes on the production history will be studied here.

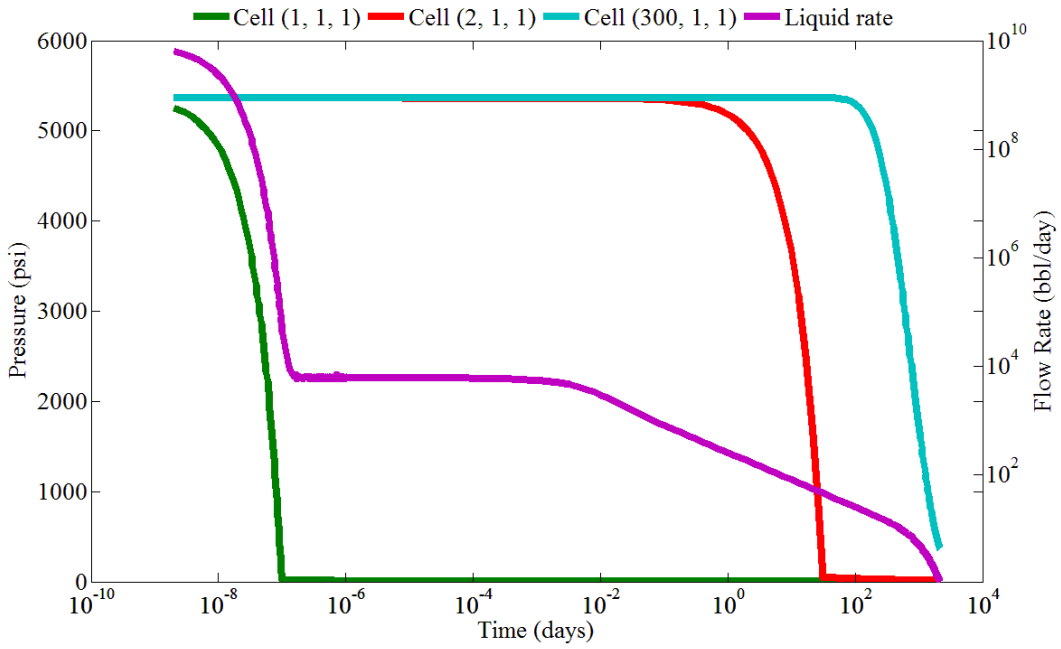

Figure 5: Production and pressure profile of single compartment model

Spreadsheet Simulations

The spreadsheet simulations show the pressure profile (Figure 6), well production history (Figure 7), and the productivity index (Figure 8).

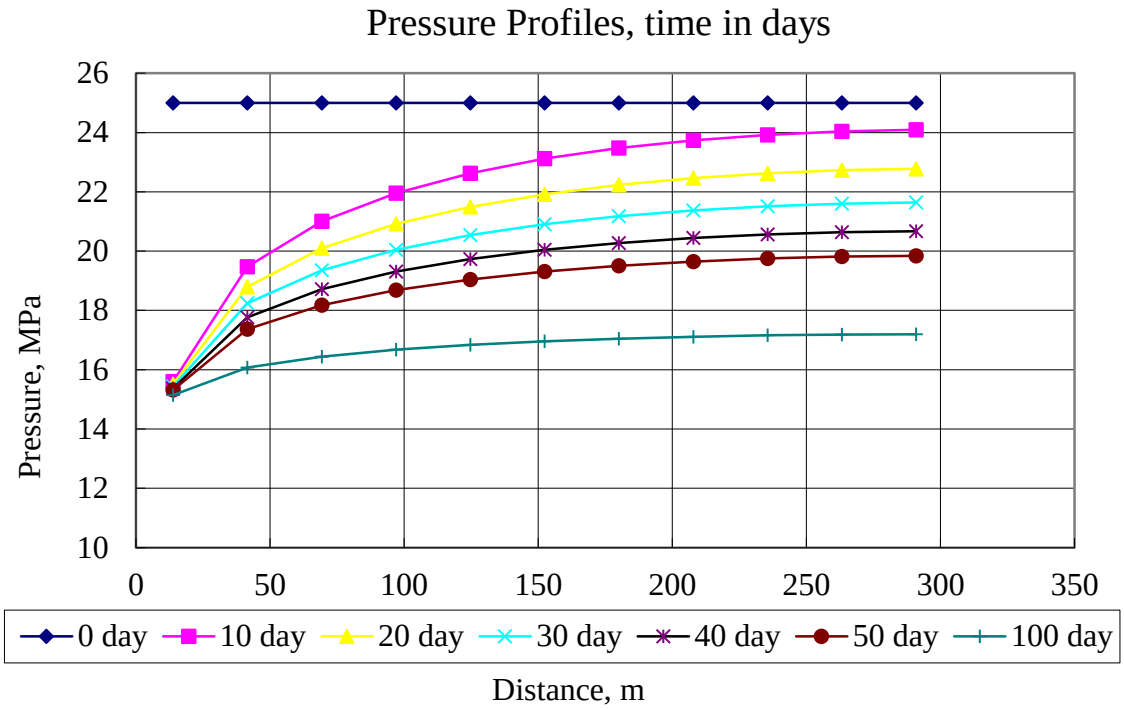

Figure 6: Pressure profile from spreadsheet simulator

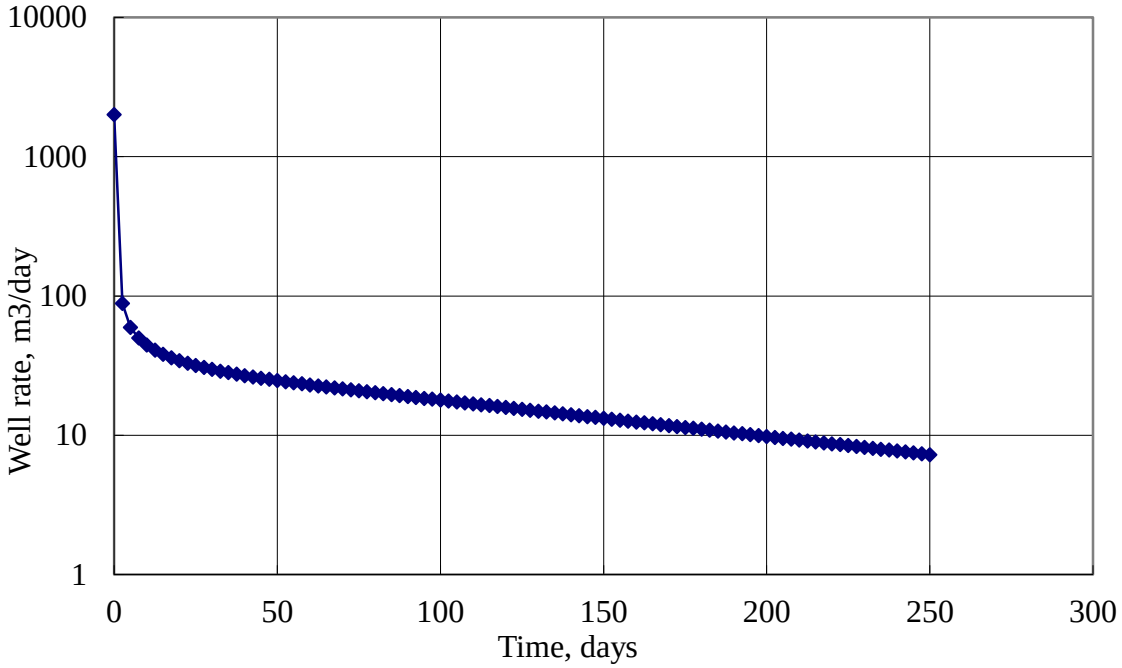

Figure 7: Production history from spreadsheet simulator

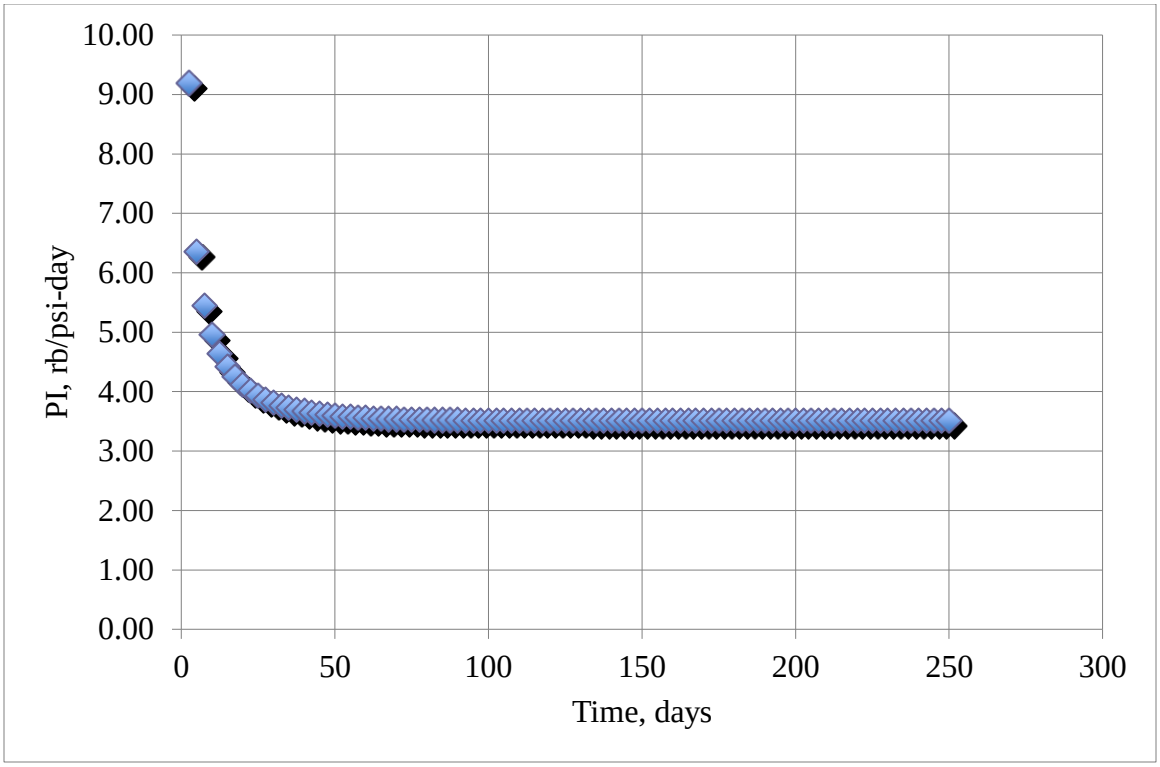

Figure 8: Productivity index from spreadsheet simulation

The pressure profile shows the change in pressure distribution throughout the reservoir with time. Initially, the reservoir pressure is uniform at 25 MPa. After the well starts to produce, the bottom hole pressure immediately drops to 15 MPa and the rest of the reservoir pressure decreases slowly but steadily. Those cells that are the closest to the wellbore drops faster than cells farther from the wellbore. Production history shows a dramatic decline in production rate in first 10 days and the later production follows an exponential decline pattern commonly observed under primary recovery. The productivity index declines significantly, and then remains constant for the rest of well life for primary recovery period.

The spreadsheet simulation results are able to capture the production performance of a well. However, the model lacks variable time steps and adjustable length of

simulation time to easily provide desired simulation data. With variable time steps, the entire production can be broken down into finer temporal resolution so that change in flow regime can be observed. Increasing length of production enables the reservoir to undergo more flow regimes. In comparison, commercial reservoir simulation has more options and will be more convenient for later analysis, so all the following reservoir simulations were done in CMG IMEX with relevant inputs specified in this chapter.

Chapter 3: Combined CRM Formulation

PROPOSAL OF COMBINED PRODUCTIVITY INDEX MODEL

El-Banbi and Wattenbarger (El-Banbi and Wattenbarger, 1998) gave an analytical solution of early time approximation of the single compartment model with constant bottom hole pressure condition. The early time approximation describes the flow behavior for the linear transient flow regime, where the fluid flow is perpendicular to the fracture face and the pressure propagates outward from the fracture, but the pressure propagation from neighboring fractures have not interfered with each other. The solution is shown in Equation 3,

$$\frac{1}{q_D} = \frac{\pi}{2}\sqrt{\pi t_{Dx_f}} \tag{3}$$

where $q_D = \frac{kh(p_i - p_{wf})}{141.2qB\mu}$ and $t_{Dx_f} = \frac{0.00633kt}{\phi\mu c_t x_f^2}$.

q_D and t_{Dx_f} are dimensionless flow rate and time. Equation 1 shows that the dimensionless flow rate is inversely proportional to dimensionless time. In field units, the relationship between flow rates the time is shown in Equation 4

$$\frac{q}{P_i - P_{wf}} = \frac{2hx_f}{141.2B}\sqrt{\frac{\phi k c_t}{0.00633\pi^3\mu t}} \tag{4}$$

where h is fracture height, x_f the fracture half length, B the oil formation volume factor, ϕ the porosity, k the formation permeability, c_t the total compressibility, and μ the oil viscosity.

It is assumed in the model that reservoir and fluid properties $h, x_f, B, \phi, k, c_t, \pi, \mu$ are independent of both time and pressure, so $\frac{q}{P_i - P_{wf}}$ is only a function of square root of time in the constant bottom hole pressure condition. Furthermore, the initial reservoir pressure is a constant, and the analytical model assume constant bottom hole pressure boundary condition, so the above analytical model states that the flow rate is a function of

square root of time. $\frac{q}{P_i - P_{wf}}$ resembles the formulation for classic productivity index, but the average reservoir pressure in the classic formulation is replaced by the initial reservoir pressure. If the initial reservoir pressure can be approximated by the average reservoir pressure, the productivity index can be analyzed as a function of time. In theory, during the linear transient regime, the pressure propagation from the wellbore is really slow so the pressure in the majority of the reservoir is unaffected remaining at the initial reservoir pressure; and thus the average pressure should be similar to the initial reservoir pressure. To check the legitimacy of the pressure approximation, a reservoir simulation producing entirely within the linear transient flow regime is needed. Figure 9 shows a reservoir simulation with permeability of 0.025 md.

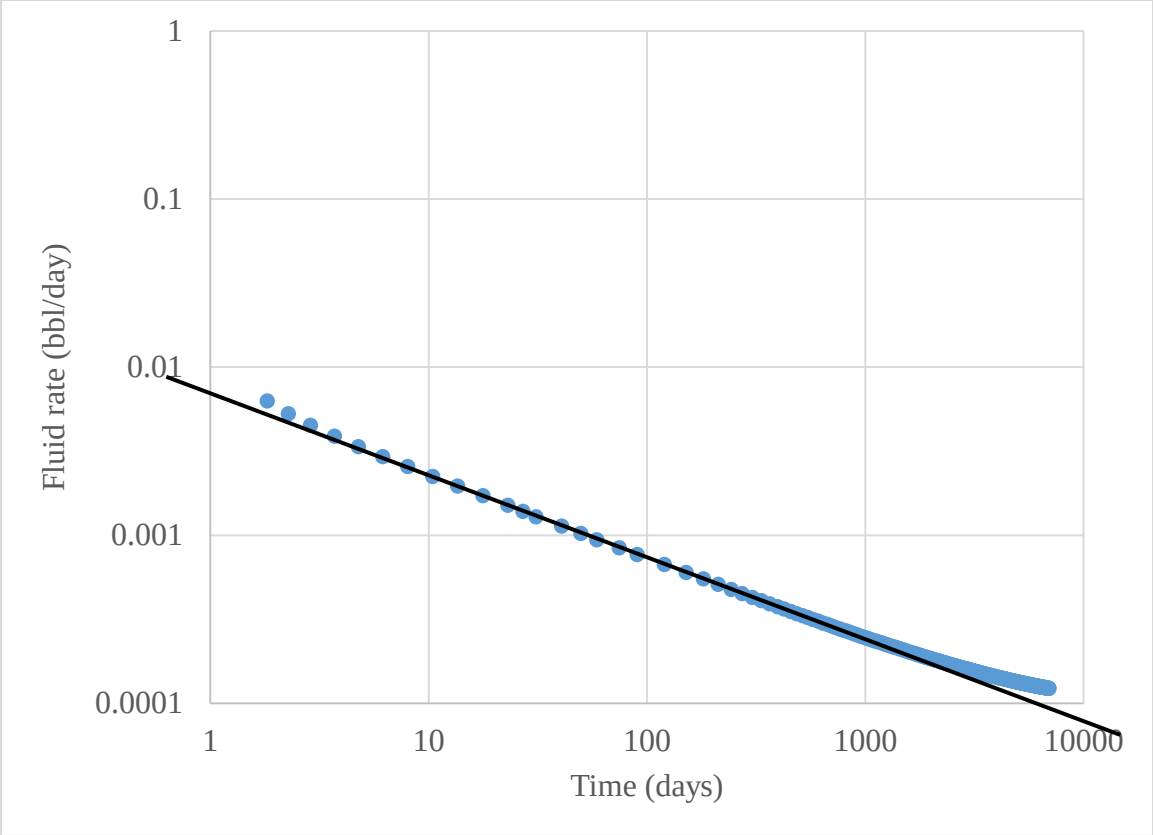

Figure 9: Production history for simulation with permeability of 0.025 md

From the plot above, the black line has a slope of one-half indicating the presence of linear transient flow (Wattenbarger and El-Banbi 1998). The majority of production data lie on the black line. Only those points after about 1000 days deviate from the black line, marking the end of linear transient flow. Since the initial reservoir pressure is approximated by the average reservoir pressure in only the linear transient flow equation, the pressure data within the first 1000 days is of most concern here. Figure 10 plots average reservoir pressure from simulation results with permeability of 0.025 md against time and compares the average reservoir pressure with the initial reservoir pressure. The initial reservoir pressure is independent of time; however, it is plotted as a constant to see how much the average pressure deviates since the start of the production. The average reservoir pressure gradually deviates from the initial pressure from the start of production. As time progresses, the deviation becomes larger and the largest deviation happens at the end of linear transient flow regime. The biggest difference between the average reservoir pressure and the initial pressure is only 12%. Such errors are not too significant to damage the pressure approximation. The percentage difference is calculated by taking the differences between two pressure values and dividing the difference by the initial reservoir pressure. So with such small permeability, the average reservoir pressure is a good approximation for initial reservoir pressure.

The same comparison using simulation data with permeability of 2.5 md is useful to analyze whether a larger permeability will have negative impacts on the pressure approximation as explained above. Figure 11 shows the initial reservoir pressure and the average reservoir pressure from a simulation with permeability of 2.5 md. The average pressure changes dramatically during the entire production history, ranging from 5300 psi to 10 psi. During the majority of the production history, the average pressure deviates significantly from the initial reservoir pressure. Table 2 shows how the pressure of cell

(300, 1, 1) changes with time. The cell pressure has minor changes from the beginning, possibly because of implicit pressure-solving algorithm, until 31 days when the pressure starts to change over 10 psi every time step. When the pressure remains relatively unchanged, the pressure from the wellbore has not propagated to the boundary, so the linear transient flow regime ends after 31 days.

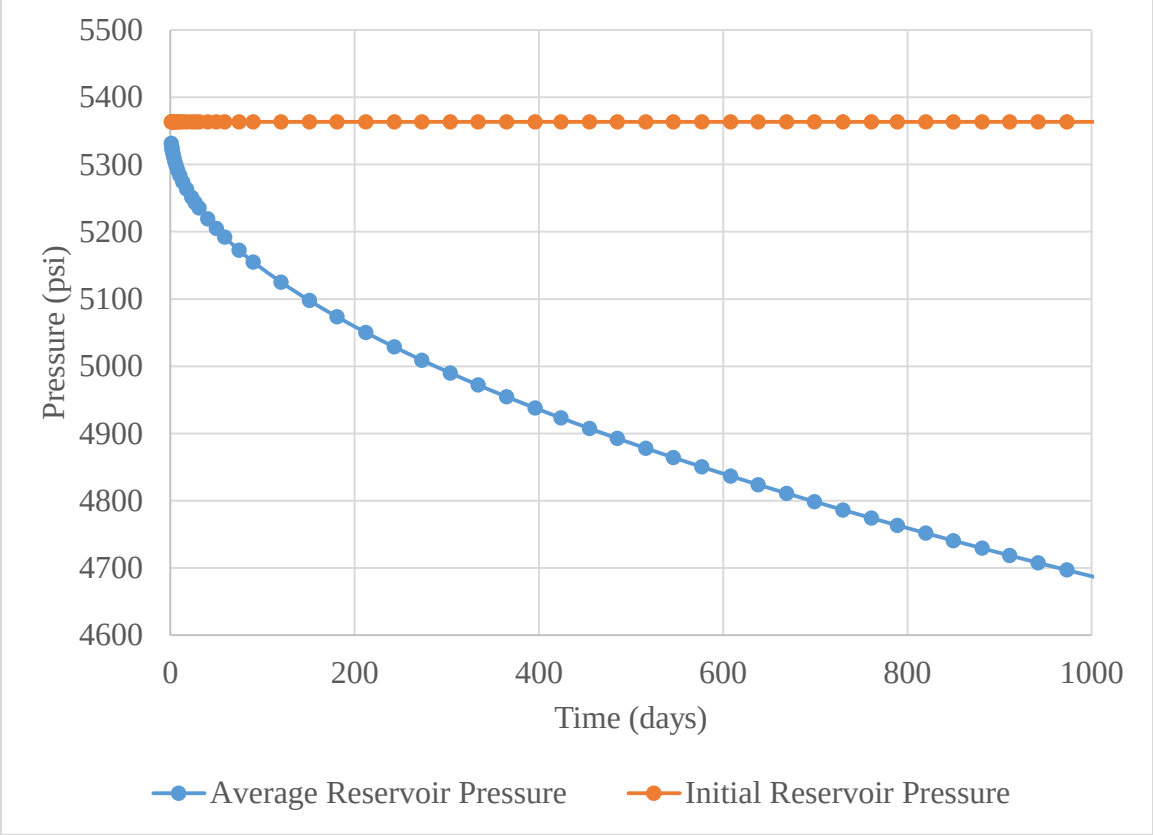

Figure 10: Comparison of average reservoir pressure and initial reservoir pressure from simulation results with permeability of 0.025 md

Figure 12 shows the pressure history within only the linear transient flow regime. By plotting these production data, Figure 12 shows that the average pressures do not deviate significantly from the initial pressure. Similar to the previous case, the deviation increases with time, but the largest deviation is only 13.9%, so the pressure

approximation makes an error that is well within engineering accuracy. So even at a higher permeability, as long as the flow is in the linear transient regime, the initial reservoir pressure can be approximated by the average reservoir pressure.

Time (days)	Cell Pressure
0.0	5363.5
0.7	5363.5
1.0	5363.4
1.3	5363.4
1.6	5363.4
2.0	5363.4
2.6	5363.3
3.3	5363.2
4.3	5363.2
5.6	5363.1
7.3	5362.9
9.5	5362.7
12.4	5362.5
16.2	5362.2
21.2	5361.7
26.1	5361.3
31.0	5360.9
40.8	5345.5
49.9	5331.2
59.0	5316.9
74.5	5251.8

Table 2: Pressure history for cell (300, 1, 1)

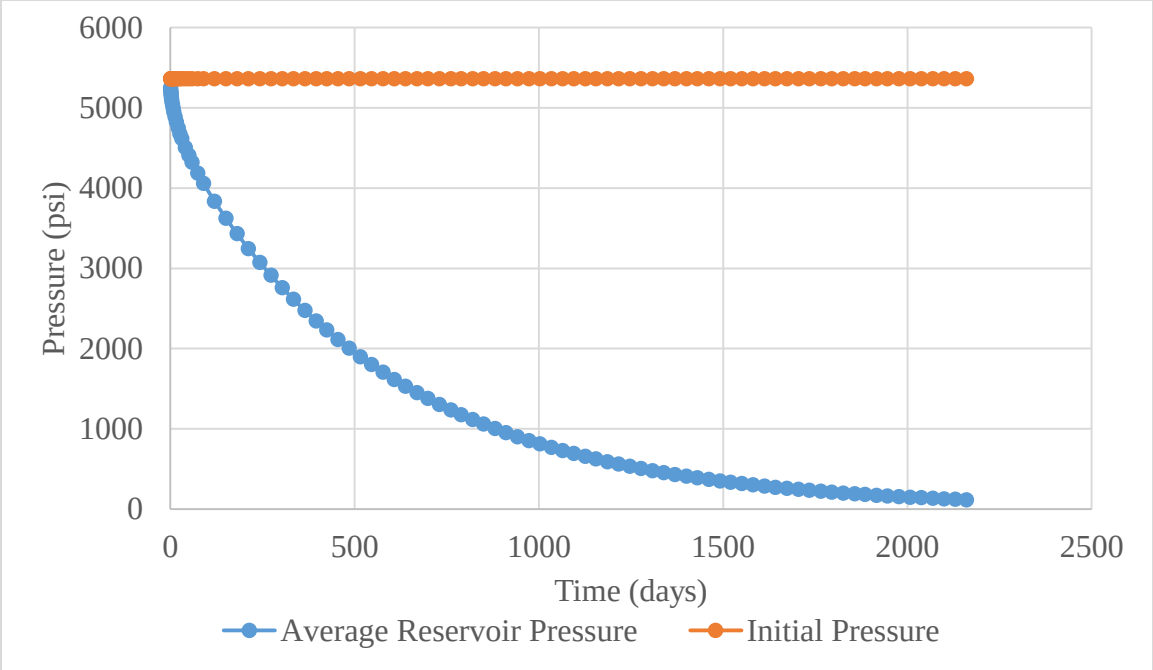

Figure 11: Comparison of average reservoir pressure and initial reservoir pressure from simulation results with permeability of 2.5 md

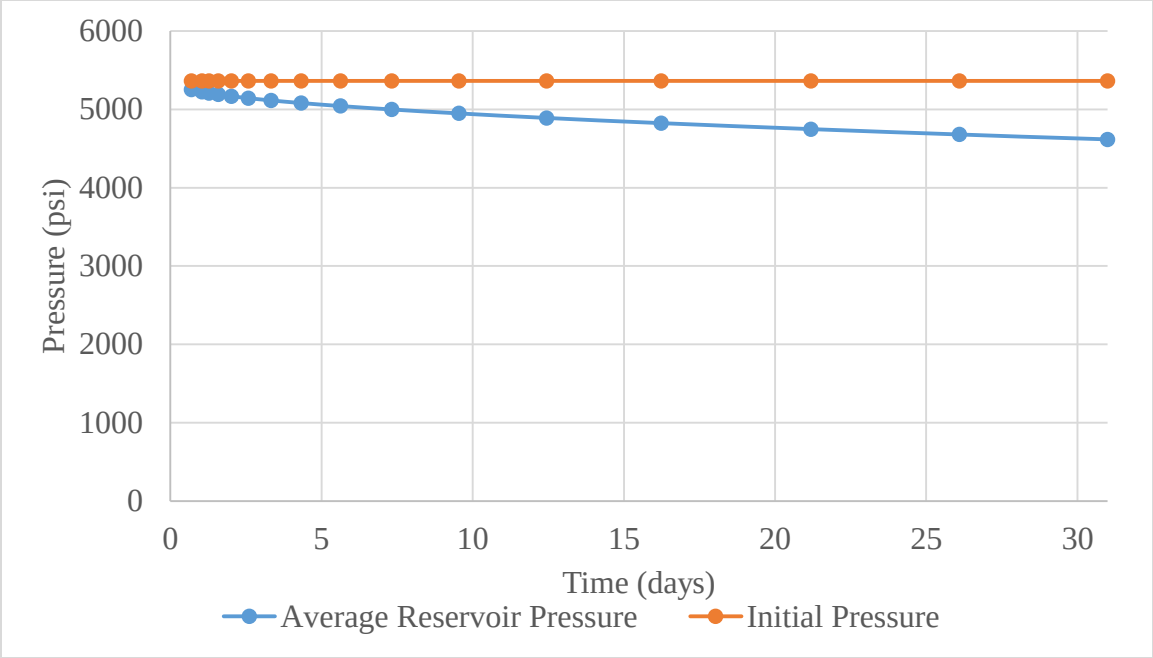

Figure 12: Comparison of average reservoir pressure and initial reservoir pressure from simulation results with permeability of 2.5 md during linear transient flow regime

As a result, the initial reservoir pressure can be approximated by the average reservoir pressure; and thus the productivity index equation for early time approximation of the single compartment model can be formulated in the same way as in the classic productivity index equation, as shown in Equation 5. Some rearrangements, as shown in Equation 6, reveal that plotting the productivity index against time will yield a line with a negative one-half slope on a log-log plot.

$$J = \frac{q}{P_i - P_{wf}} = \frac{\beta}{\sqrt{t}} \tag{5}$$

$$\log(J) = \log(\beta) - \frac{1}{2}\log(t) \tag{6}$$

Where $\beta = \frac{2hx_f}{141.2B}\sqrt{\frac{\phi k c_t}{0.00633\pi^3\mu}}$, and $J = \frac{q}{\bar{P}-P_{wf}}$

Single-compartment simulation results from Chapter 2 were used to verify the above theory. In Figure 13, the production rate declines with a half-slope on a log-log

plot indicating the entire production is within the linear transient flow regime. The productivity index is also plotted on the same graph showing a half-slope, which confirms that the initial reservoir pressure can be approximated by the average reservoir pressure in computing the productivity index for early stage production. In addition, it validates the productivity index model for linear transient flow.

As the permeability is increased to 0.75 md in Figure 14, both productivity index and production rate show a half-slope behavior for the first 100 days; however, productivity index then flattens out while the production rate takes a steeper turn.

The well performance after 100 days can be seen more clearly on a semi-log plot as in Figure 15, where the production rate takes on an exponential decline and the productivity index remains constant. The key point is that the productivity index is inversely proportional to the square root of time for the transient linear regime but will transition to a constant value as the fractures start to interfere. As a result, the following model is proposed to capture the production index behavior for the single compartment model over both linear transient and semi-steady state flow:

$$J = \frac{\beta}{\sqrt{t}} + J_{\infty} \tag{7}$$

The first part of the model represent the early linear transient flow and the J_{∞} represents the constant productivity value that the well will eventually reach. At the early time, the first term will dominate, since the time is in the denominator, while later on the second term will dominate as time progresses in that time has less impact on productivity index at later time.

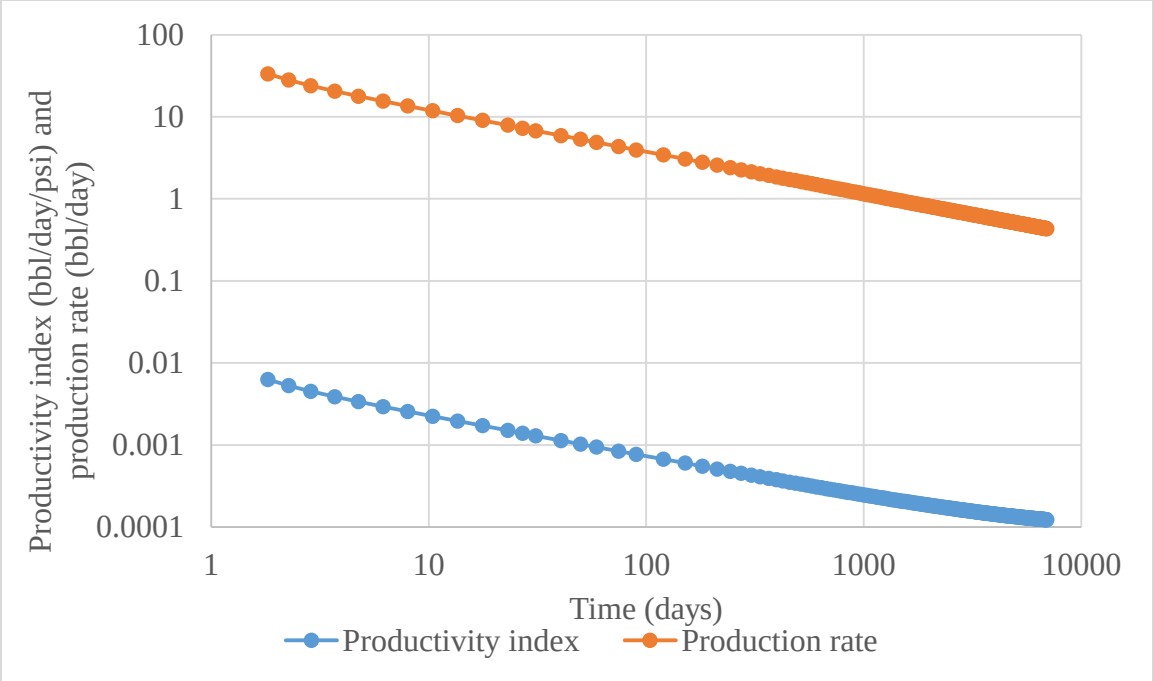

Figure 13: Productivity index and oil rate vs. time from simulation with permeability of 0.025 md

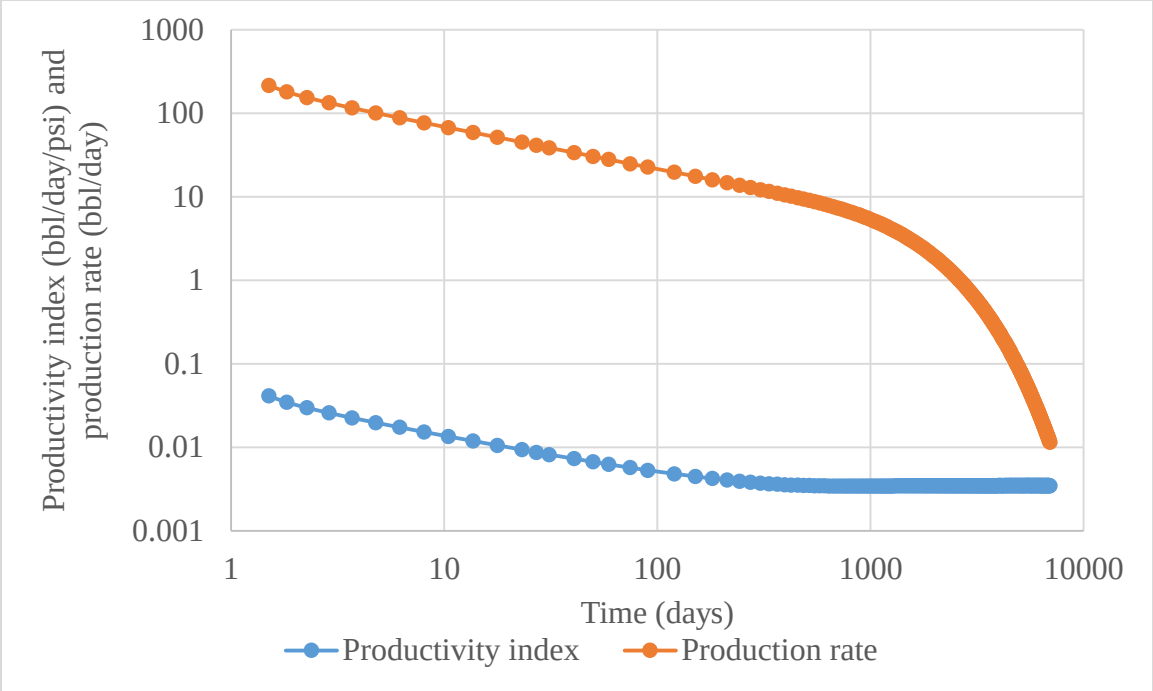

Figure 14: Log-log plot of productivity index and oil rate vs. time from simulation with permeability of 0.75 md

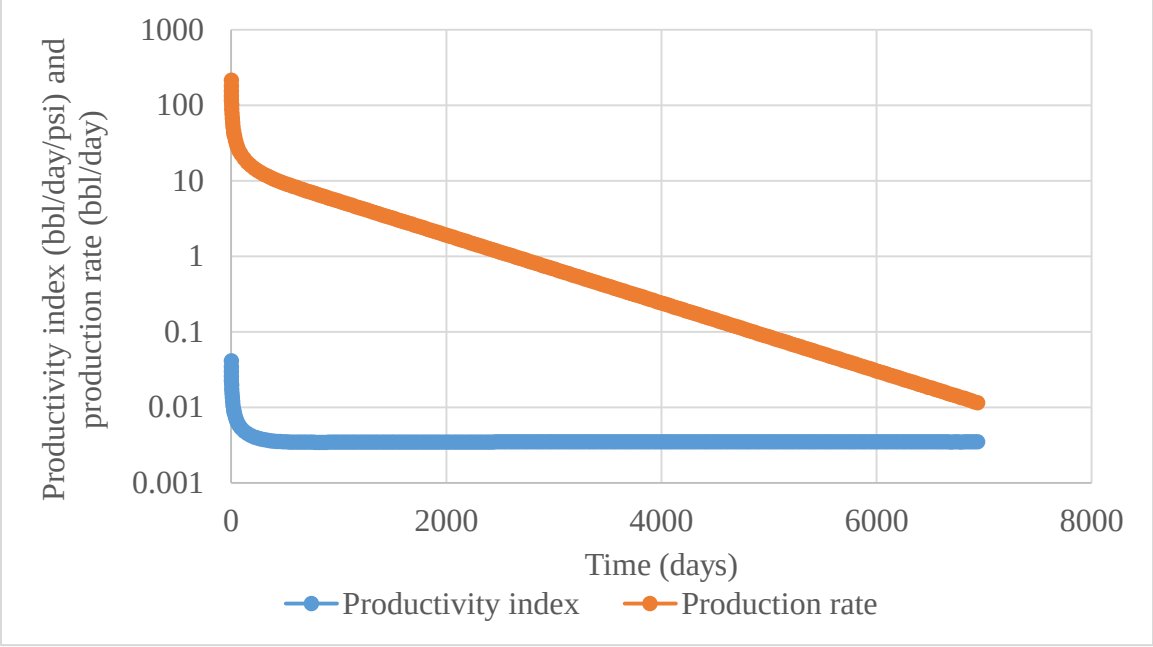

Figure 15: Semi-log plot of productivity index and oil rate vs. time from simulation with permeability of 0.75 md

The above results are based on constant bottom hole pressure, and it is also insightful to examine the flow behavior when the bottom hole pressure changes as a step-wise function.

A reservoir simulation with permeability of 0.075 md was conducted. Instead of keeping the bottom hole pressure as a constant throughout the production history, the pressure was first kept at 1000 psi, and then was changed instantaneously to 100 psi in 32 days. The pressure history for cell (300, 1, 1) and the bottom hole pressure changes are plotted on Figure 16.

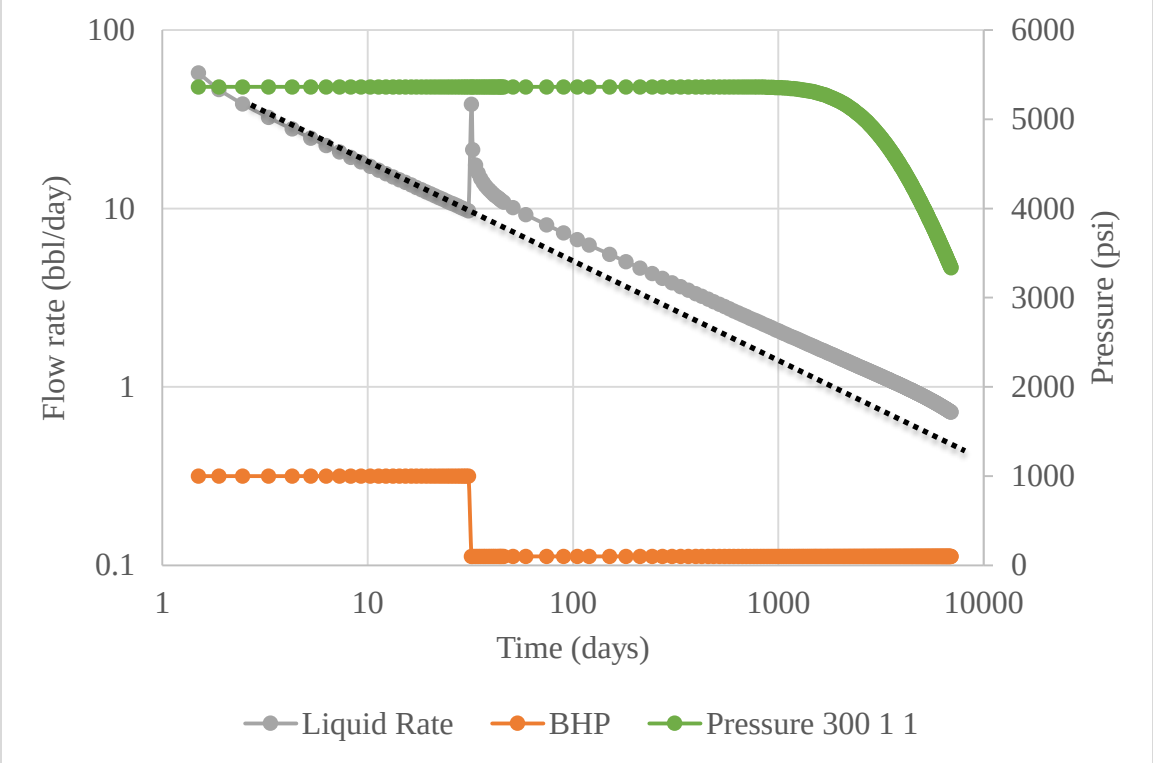

Figure 16: Pressure and production performance with step-wise bottom hole pressure change. (0.075 md)

From the above pressure history, the pressure at the outer boundary remains constant until about 1000 days, which indicates the end of transient linear flow regime.

The production rate shows a half-slope on a log-log plot, indicated by the dashed black line, when the bottom hole pressure was kept at 1000 psi. When the bottom hole pressure is changed from 1000 psi to 100 psi, there is a significant production increase response. The production rate instantaneously increases from 9 bbl/day to 38 bbl/day, but declines gradually back to 9 bbl/day in 28 days. Then, the production rate resumes its half-slope behavior for the rest of the production history. However, the production performance is constantly above the black dotted line after the change in bottom hole pressure, so the pressure perturbation shifts the half-slope production history upward and permanently alters the flow behavior. The pressure perturbation introduces a "transient" regime within the original linear transient flow regime.

Figure 17 shows the productivity index behavior for this simulation. Similar to the previous results, the productivity indices before and after the pressure perturbation show the same half-slope, indicated by the black dashed line. However, instead of showing an upward shift, the productivity index data after pressure perturbation remains on the same trend line as they lie on the black dotted line. The productivity index behavior after 1000 days deviates from half-slope, because the pressure propagation has reached the boundary of the reservoir, as shown on the cell (300, 1, 1) pressure profile. So the deviation marks the end of the transient linear flow.

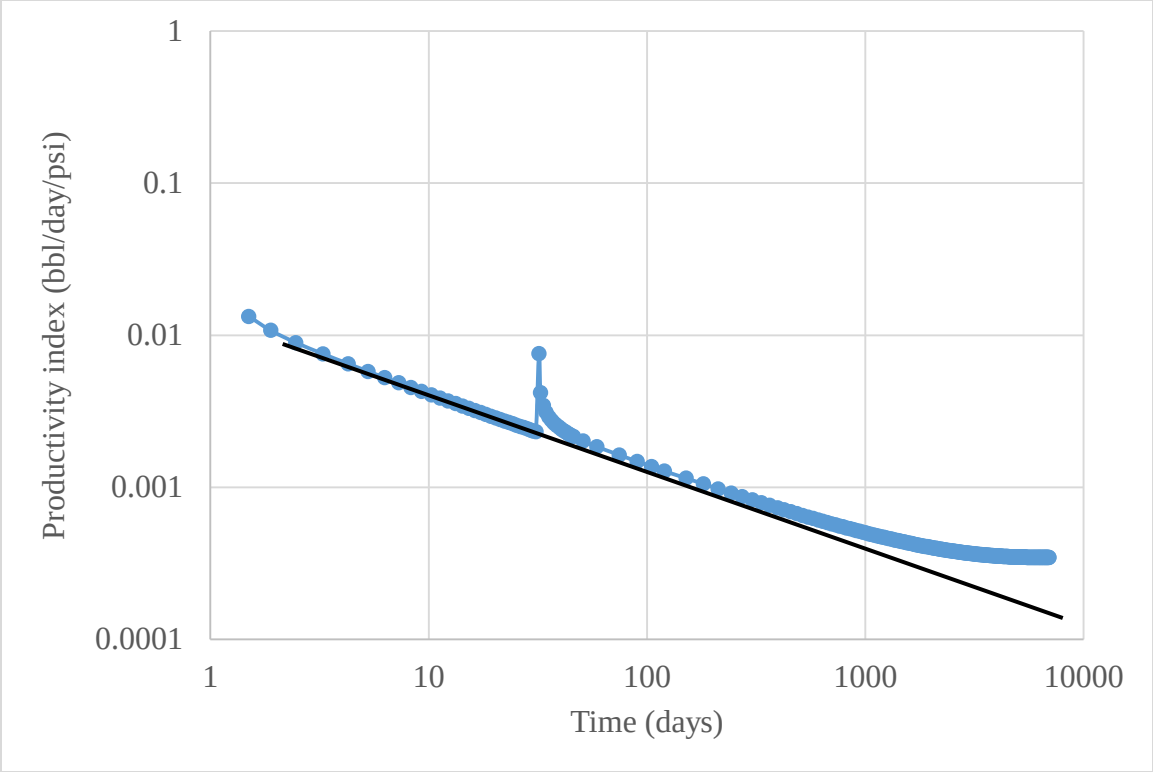

Figure 17: Productivity index performance with step-wise bottom hole pressure change (0.075 md)

Similarly, a pressure perturbation is introduced to a production history for a well predominantly in semi-steady state flow. A reservoir simulation with permeability of 10 md was conducted. The behavior is shown in Figure 18. The bottom hole pressure is kept at 1000 psi for the first 1000 days and then changed to 100 psi. The cell (300, 1, 1) pressure starts declining from the very beginning of the production, indicating minimal linear transient flow period. Before the pressure perturbation, the production history shows a significant period of exponential decline. On the 1000th day, the cell (300, 1, 1) pressure responses immediately to the pressure perturbation from the bottom hole, and the production rate spikes from 0.002 to 40 bbl/day. Then, the production rate resumes its

exponential decline from the new production rate. The slopes of the exponential decline are the same.

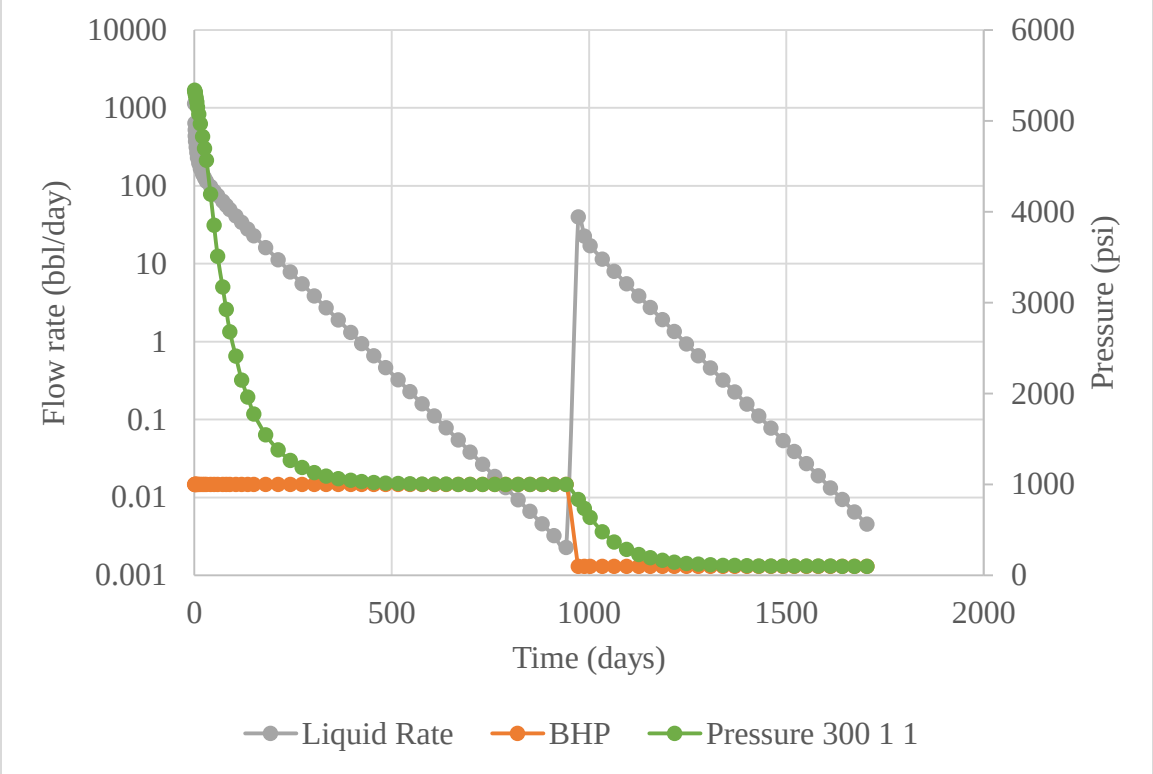

Figure 18: Production and pressure response from step-wise bottom hole pressure (10md)

The productivity index behavior for the same simulation is shown in Figure 19. Since the start of the production, the production rate declines dramatically. Then, the productivity index remains constant. Reducing the bottom hole pressure on the 1000th day instantaneously increase the productivity index, which however drops back to its previous level immediately.

In conclusion, the changes in the bottom hole pressure have a larger impact on the production history, and have very little impact on the productivity index of the well. On production history plot, the pressure perturbation will offset the production rate to a new starting point, and then the production history will follow the same production trend. If

the permeability is very small as shown in Figure 17, it will go through a transition phase first before the production gets back to its original trend while for a large permeability case as shown in Figure 19, the production is immediate back to its prior trend after the pressure perturbation. The key point is that the production history trend remains the same, but it restarts from the offset value. In comparison, the pressure perturbation changes neither the productivity index trend nor the values in long term. It alters the productivity index behavior temporarily, which then gradually goes back to its previous value and trend as shown in both Figure 17 and 19.

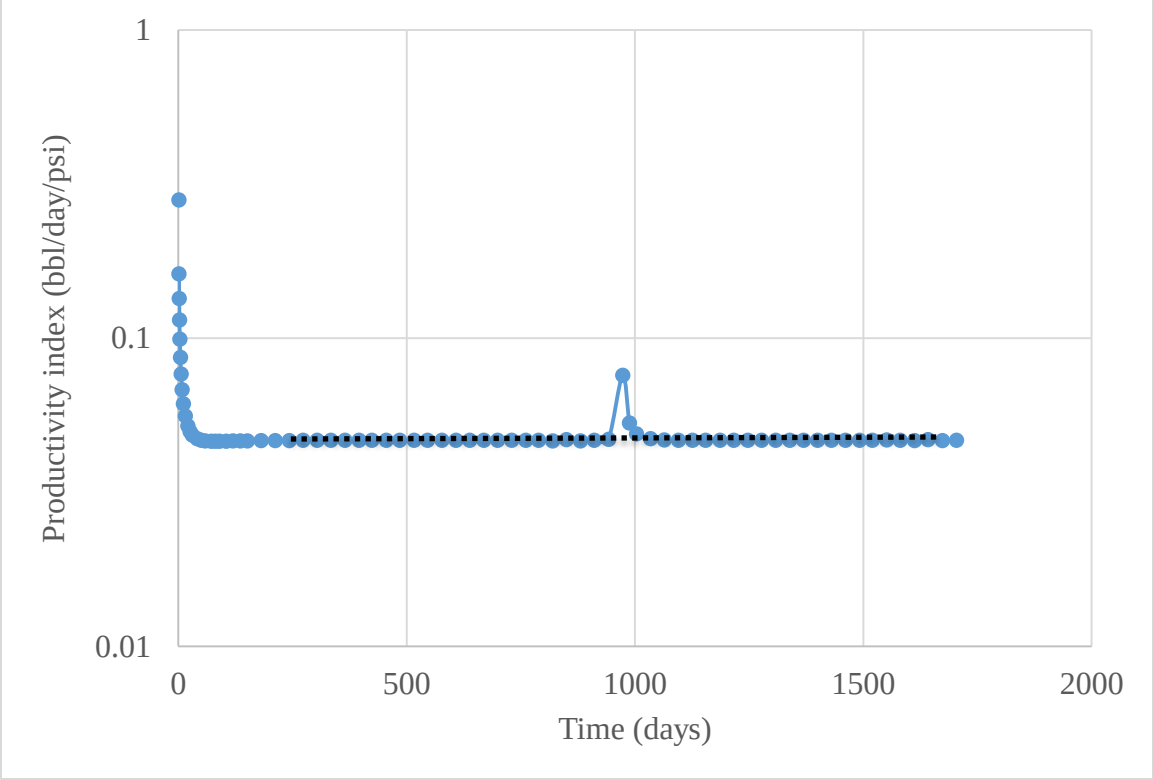

Figure 19: Productivity index behavior for step-wise change bottom hole pressure

VALIDATION OF COMBINED PRODUCTIVITY INDEX MODEL

The validation of the combined productivity index model is accomplished with the help of the Microsoft Excel Solver add-in to obtain a data match. The results of the

single compartment model simulation from last chapter is used as the history data. The modeled productivity index is calculated by first choosing reasonable values for model parameter β and J_∞. The model parameters in combination with time outputs from the simulation are used to calculate the productivity index for each time step. Lastly, the sum of squared errors between the simulated and calculated productivity index is calculated and then solver was run to minimize the sum of the errors to obtain a match, as shown in Figure 20. The percentage errors in the following plots are calculated by dividing the difference between the modeled values and the simulated values.

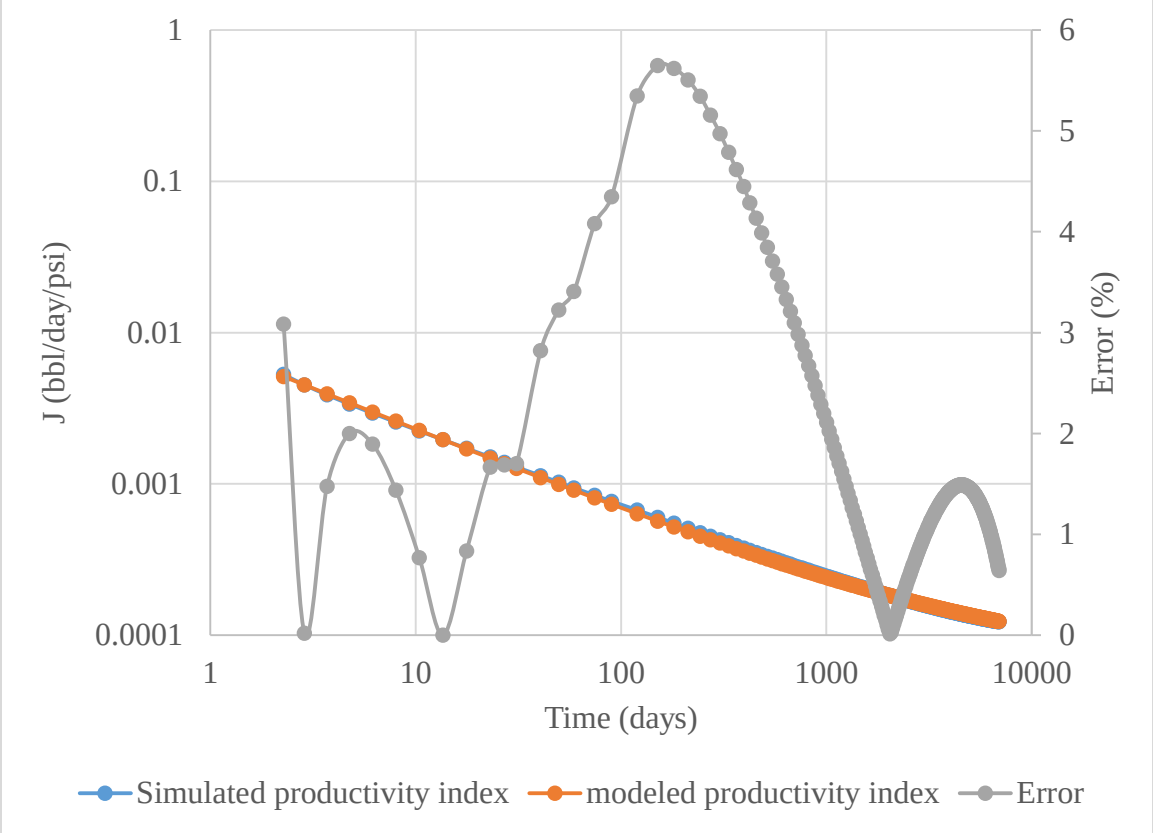

Figure 20: Synthetic history match for combined productivity index model (0.025 md)

The proposed model is able to match well the production data from linear transient flow. The maximum error percentage is merely 6% and the majority of match

remains under 3%. However, the quality of the match is different if a portion of fracture-dominated flow regime is included in the data by slightly increasing the permeability of the reservoir simulation, as shown in Figure 21.

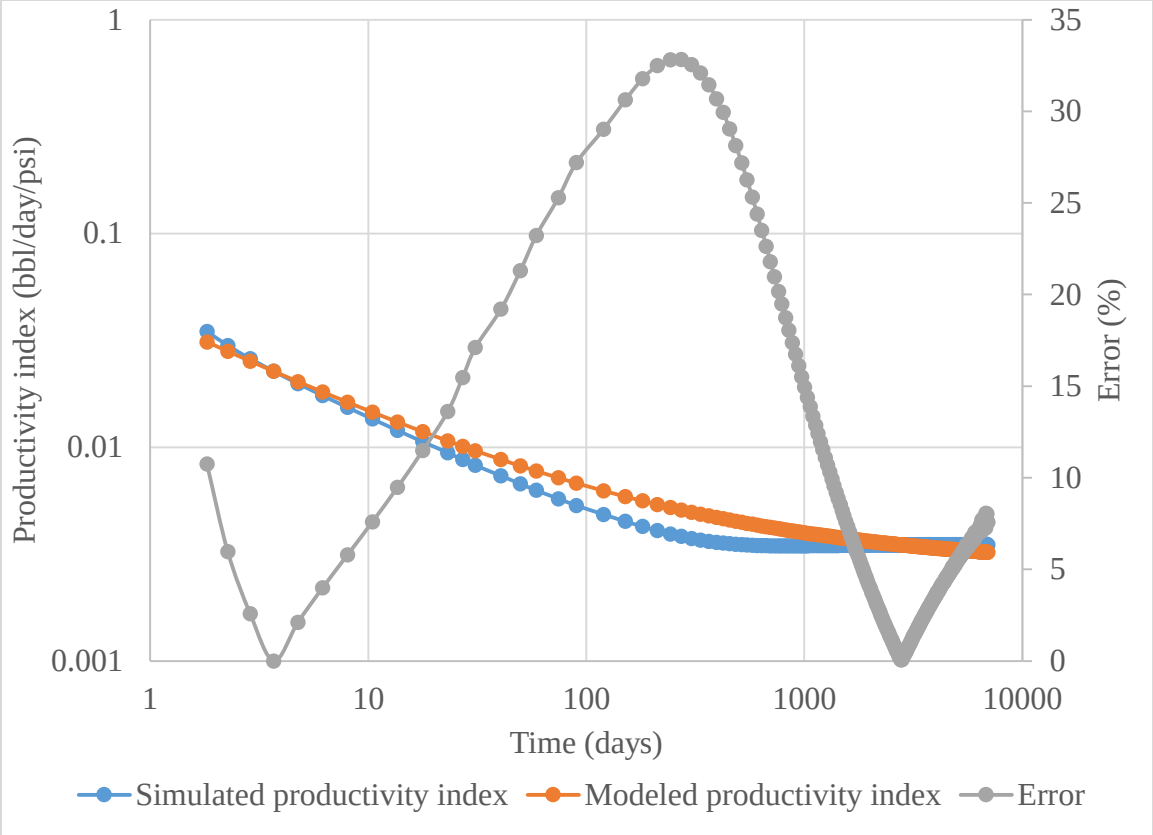

Figure 21: Synthetic history match for combined productivity index model (0.75 md)

The largest errors occur when the flow regime is in a transition period. Since the model consists of two distinct components characterizing both fracture interference and linear transient regimes, it is difficult for the model to fully match the transition. To tackle the difference between the model and the simulation data, it is proposed to make the exponential component of time also a fitting parameter, as shown in Equation 8.

$$J = \frac{\beta}{t^{\frac{1}{n}}} + J_{\infty} \tag{8}$$

The idea is that the exponent will provide the model with certain degree of flexibility to mitigate the offset during the transition. With fixed n component, the percentage errors reach up to 35%. In comparison, changing n component to a fitting parameter reduces the maximum error from 35% to 16%. As shown in Figure 22, n as a fitting parameter makes the production history much better.

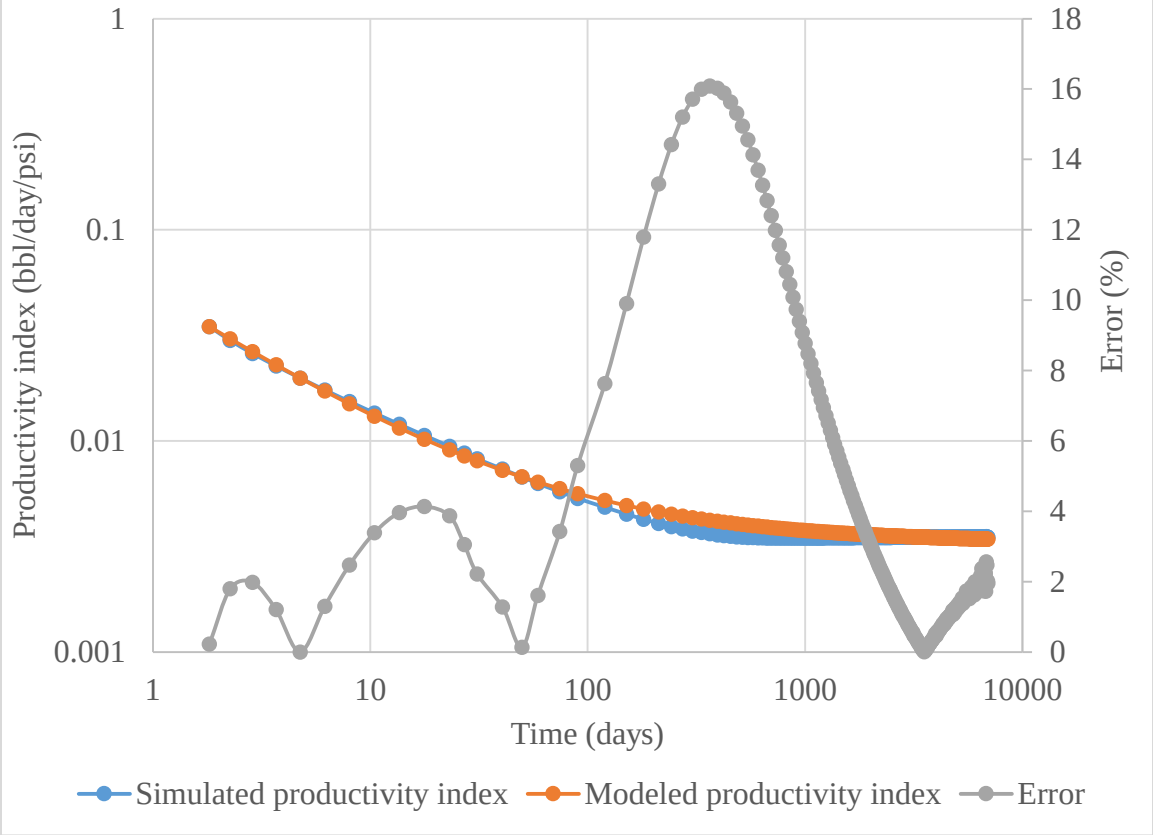

Figure 22: Synthetic history match for combined productivity index model after changing the exponent (0.75 md)

SENSITIVITIES OF COMBINED PRODUCTIVITY INDEX MODEL TO FITTING PARAMETERS

It is important to examine how different values of fitting parameters in the combined productivity index model affect the productivity index behavior, and such

analysis will assist in understanding how this model reflects the physics of fluid flow in both linear transient and semi-steady state flow regime.

Equation 7 and the associated definition of β offer the opportunity to calculate the productivity index at each time step with given steady state productivity index as well as fluid and reservoir properties, such as compressibility, viscosity, etc. The default values for steady-state productivity index is 2×10^{-2} bbl/day/psi, β is 1.22×10^{-1} bbl/day$^{1/2}$/psi, $c_t V_p$ is 6.42 and n is 0.7. Figure 23 shows the effect of various steady state productivity index on the combined productivity index. While keeping all other parameters the same, three logarithmically spaced steady-state productivity index values are chosen ranging from 1×10^{-4} to 1×10^{-2} bbl/day/psi.

As emphasized in the previous section, the steady-state productivity index is a characteristic of the steady state flow regime. The larger the value, the more dominant the steady-state regime is as shown in the Equation 7. If the steady state productivity index, which is the second term in Equation 7, is dominanting, then the effect of the first term representing the linear transient regime is completely negligible. In that case, the combined productivity index will be independent of time and shows a constant value over time. On Figure 25, the combined productivity index when J is 1×10^{-3} bbl/day/psi is mostly constant and does not vary with time. When the steady state productivity indices become smaller, as represented in red and green curves, the combined productivity indices are no longer constant, because the time dependent component in the productivity index model becomes more significant.

Figure 24 demonstrates the effect of β on the combined productivity index. Contrary to the effect of steady state productivity index, the larger β value, the more significant the linear transient regime. As shown in Figure 26, the blue curve shows time

dependent combined productivity index behavior, simply because the β value of the blue curve is bigger, which makes the time dependent term more pronounced.

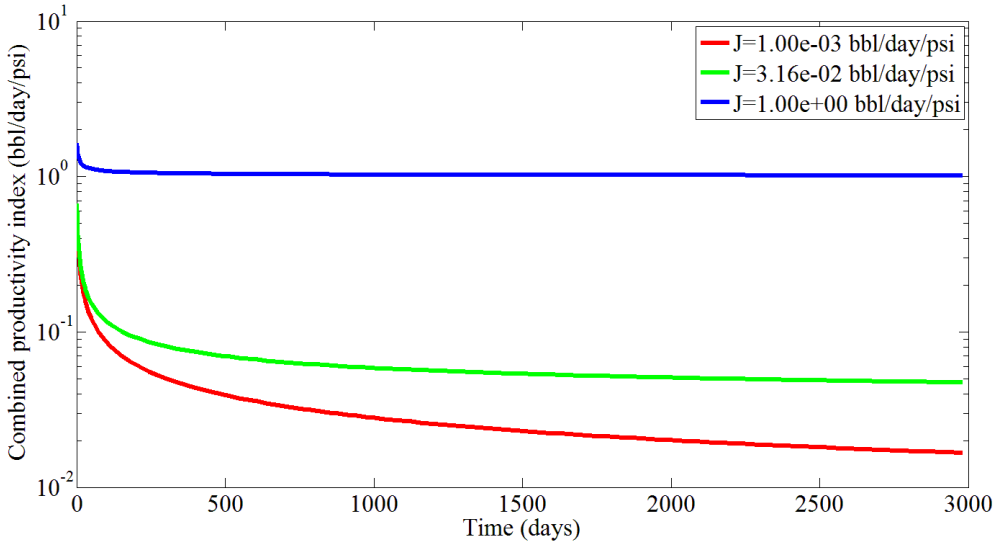

Figure 23: Combined productivity indices calculated with various steady state productivity indices

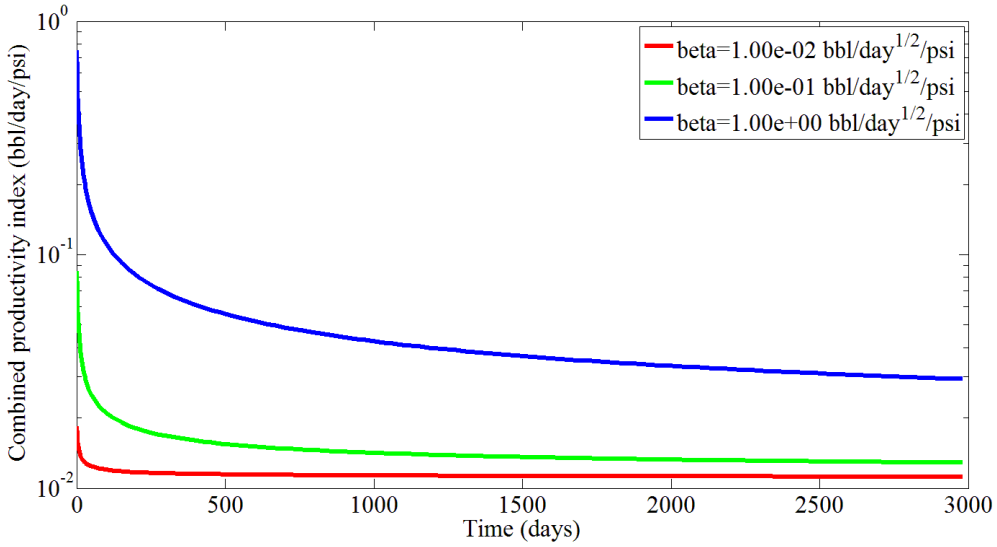

Figure 24: Combined productivity indices calculated with various beta values

COMBINED CRM TO MATCH SYNTHETIC HISTORY DATA

After validating the combined productivity index equation, the next step is to incorporate the model into the fundamental equation of CRM to derive a mathematical description of flow rate as a function of time.

The fundamental equation of CRM is a material balance differential equation (Equation 9),

$$V_p c_t \frac{d\bar{P}}{dt} = -q \tag{9}$$

which describes a relationship among pressure, rate and time. To use CRM for history matching and production forecasting, Equation 9 must be coupled with a pressure-rate relationship so that the pressure term can be eliminated. To achieve this, the steady state productivity index equation is used to derive an unsteady state CRM. During transient flow, the proposed combined productivity index equation will achieve the same goal. By rearranging Equation 8, we obtain

$$q = -(J_\infty + \frac{\beta}{t^n})(\bar{P} - P_{wf}) \tag{10}$$

By inserting Equation 10 into Equation 9 and integrating (details in Appendix A), flow rate as a function of time is derived,

$$q = J_\infty (P_i - P_{wf}) \left(1 + \frac{\beta}{J_\infty t^n}\right) e^{-\left(\frac{t}{\tau} + \frac{\beta}{(1-n)ctV_p} t^{1-n}\right)} \tag{11}$$

To validate the model, the single compartment model simulation result is fitted with the above equation in the same way that the productivity index equation was fitted in the previous chapter. The results are in Figure 25, which is a simulation case with permeability set to be 0.025 md. The permeability is chosen so that the entire production profile is within the linear transient flow regime. A good match between the modeled data and simulation results is obtained. The biggest advantage of the combined CRM is that the combined productivity index model is derived from the analytical solution to the

single compartment geometry. As a result, the fitting parameters in the combined CRM all have physical meanings, and they reveal some very important reservoir properties. Table 3 lists the reservoir parameters from the simulation inputs and those derived from the combined CRM.

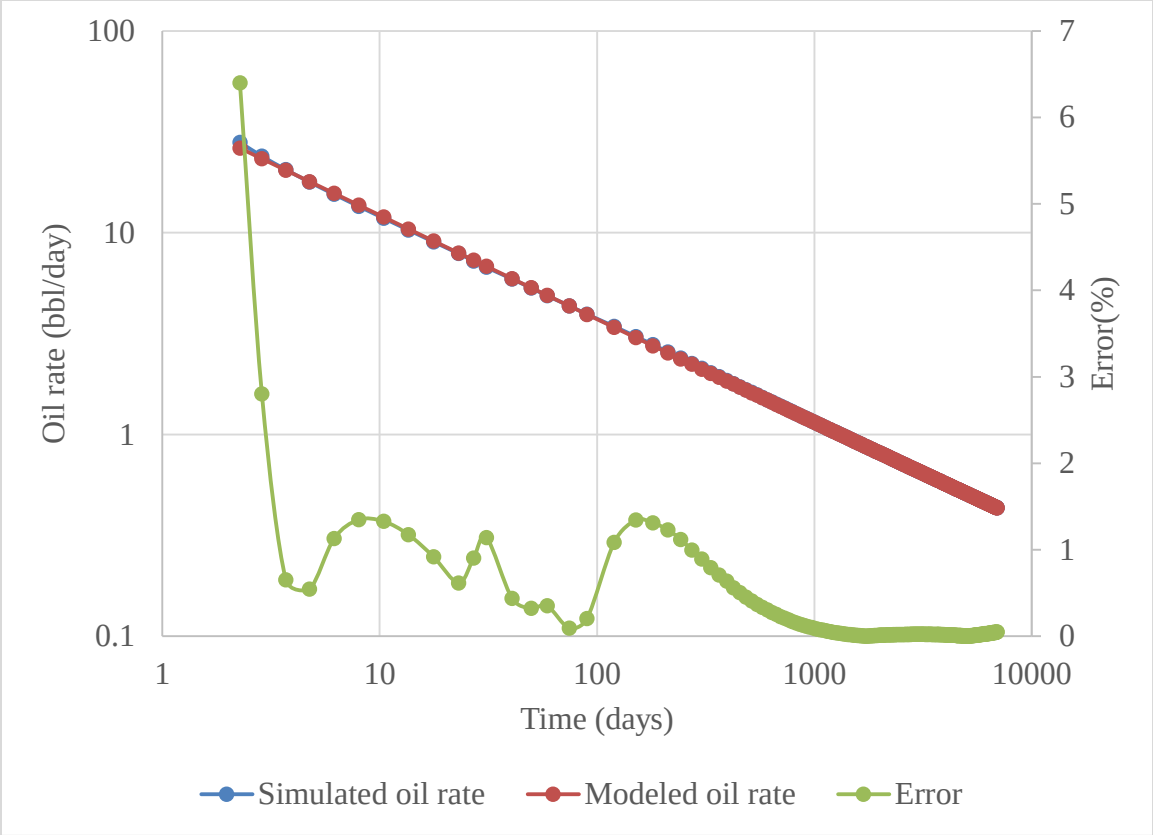

Figure 25: Combined CRM fit with simulation results for permeability of 0.025 md

	Fitted parameters	Simulation inputs/analytical solutions
J (bbl/day/psi)	7.08×10^{-6}	1.23×10^{-4}
β (bbl/day$^{1/2}$/psi)	2.3×10^{-3}	8.54×10^{-3}
n	-0.53	-0.5
$c_t V_p$ (bbl/psi)	1.79	3.99

Table 3: Comparison of modeled and known parameters (0.025 md)

From the above comparison, the best parameter fit is n=-0.53. During the linear transient flow, the n parameter should be equal to -0.5, which is very close to the analytical solution. The units of beta depends on the exponent of n. If n is fixed at -0.5, then the unit is bbl/day$^{1/2}$/psi.

On the other hand, differences exist among other parameters. The reasons are twofold. First, there will always be uncertainties in model fitting. No model can estimate the exact values of a parameter; however, a good model can provide a reasonable guess that is close enough to the actual value within a certain degree of tolerance. Second, the parameters in the combined productivity index model are characteristic of a particular flow regimes respectively. The first component in the combined productivity index equation is a characteristics of linear transient flow regime while the second component is that of semi-steady state flow regime. Either component can fit production history under only their respective flow regimes really well. However, when the entire combined productivity index model is used to fit a production history with both regimes, the fitting parameters cannot be as accurate as those from fitting to individual regime, since the linear combination mode is not sophisticated enough and certain degree of comprises have to be made to fit the history.

The most significant difference in the comparison table is J_∞, the steady state productivity index, and the possible explanation is that the productivity index is a productivity measurement dominant in the boundary-dominated flow; however, the above simulation was engineered that the entire production is in linear transient flow, so without production data in semi-steady state regime, the prediction of productivity index is not expected to be accurate.

A reservoir simulation is conducted to create a production history with significant amount of production data in both linear transient regime and semi-steady state flow

regime. Figure 26 and 27 show the simulation fitting results with permeability of 2.5 md on different scales. On this log-log plot of production rate, a linear behavior indicates the linear transient flow regime while a linear trend on a semi-log plot shows the semi-steady state flow because of the constant pressure boundary condition induced by the pressure interference from the neighboring fracture. From the plots, the combined CRM model fits the simulation data really well with minimal errors. The production rates from the model are generally less than 10 % different from the history data. The errors are larger in the first 100 days, reaching up to 14%, while the model obtains a nearly perfect match with the rest of the production data. Furthermore, the errors are not stable from the start oscillating between 0% and 10%, and at later stage the errors almost remain constant. One possible explanation for this phenomenon is insufficient data from linear-transient regime. The majority of the production data are within the semi-steady state flow, so the model tries to fit the production rate at later stage while compromising the fitting quality for early data. Overall, the fitting quality is excellent.

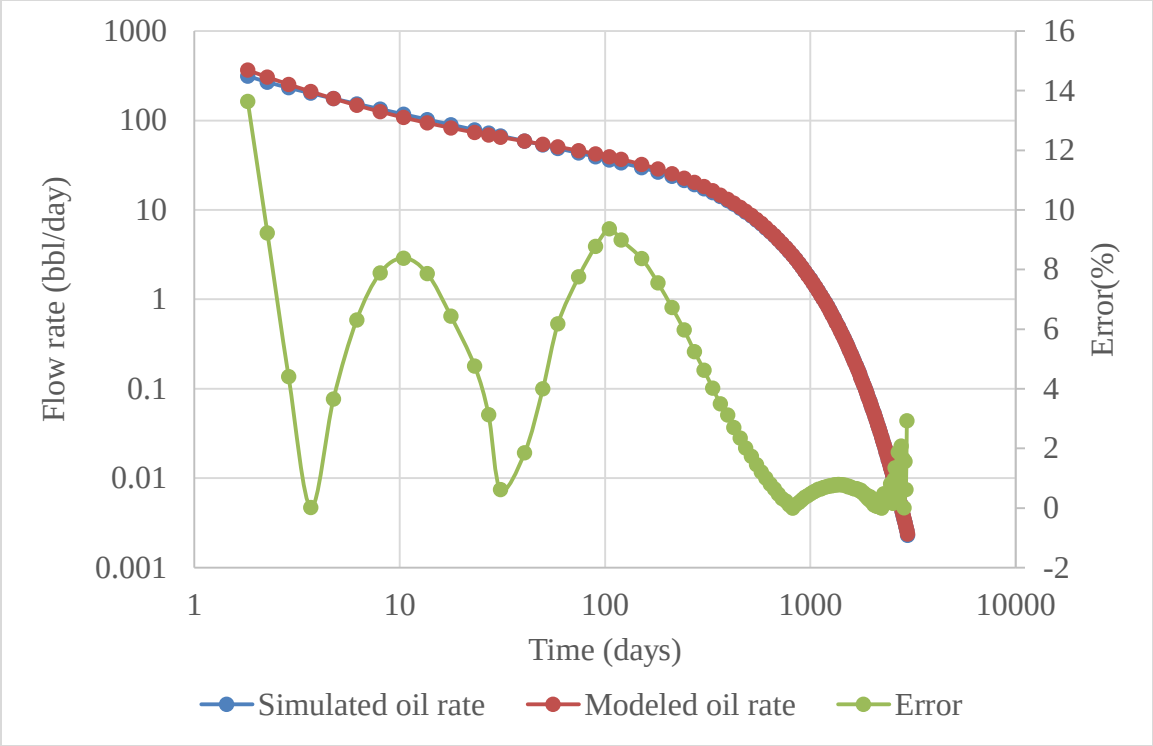

Figure 26: Combined CRM fit with simulation results (log-log plot and permeability of 2.5 md)

The parameters comparison is shown in Table 3. Different from the case with permeability of 0.025 md, the n value from the model is very different from the analytical solution while J is much closer to the simulation inputs than in the previous case. This result further reinforces the claim that when there are sufficient data for a specific flow regime, the characteristic parameter for this regime can be modeled more accurate than others.

The combined CRM model is based on the combined productivity index equation that includes a component representing the productivity behavior for linear transient regime and another component representing the behavior for semi-steady state flow. In Equation 7, the linear transient flow regime component can be easily eliminated by forcing the value of β to be zero. Furthermore, since the combined CRM model is based

on the combined productivity index, the reduction of β to zero will lead a dramatic simplification to the formulation of combined CRM model, as shown in Equation 12. The remaining equation describes the production performance for a well under semi-steady state flow regime.

$$q = J_{\infty}\left(P_i - P_{wf}\right)e^{-\frac{t}{\tau}} \tag{12}$$

where

$$q_i = J_{\infty}\left(P_i - P_{wf}\right) \tag{13}$$

By eliminating the characteristic component of linear transient regime, the combine CRM model is reduced to a semi-steady state model equivalent to commonly known exponential decline model for well under primary recovery.

	Modeled parameters	Simulation inputs/analytical solutions
J (bbl/day/psi)	0.0205	0.0110
β (bbl/day$^{1/2}$/psi)	0.122	0.85
n	-0.7	-0.5
$c_t V_p$ (bbl/psi)	6.42	3.99

Table 4: Comparison of modeled and known parameters (2.5 md)

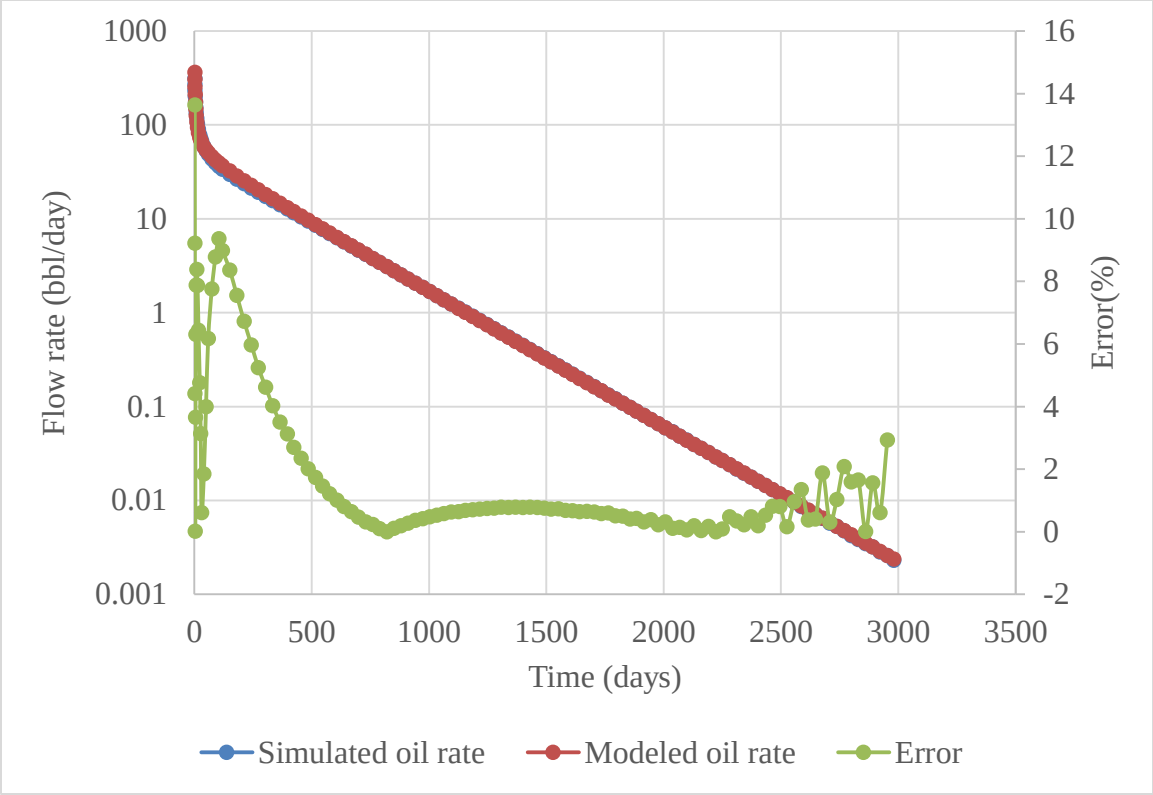

Figure 27: Combined CRM fit with simulation results (semi-log plot and permeability of 2.5 md)

THE ANALYSIS OF β AND PERMEABILITY RELATIONSHIP

According to the definition of β in Equation 6, β is linearly proportional to the square root of the formation permeability assuming that the reservoir and fluid properties in Equation 6 are constant. Such a linear relationship is investigated in this section to assist in understanding the proposed combined productivity index model.

The actual permeability values are easily accessible, since they are just inputs to simulate the production history used in previous and following chapters. The square root of those permeability inputs will be used to check the correlations. There are three ways to calculate the β values. First, β is a parameters derived based on the analytical solution to the linear transient flow regime. According to Equation 5, under linear

transient flow regime the combined productivity index and the inverse of the square root of time observes a linear relationship. If only the linear transient flow portion of the production history is used to plot such relationship, β will be the slope of the straight line. Second, Equation 6 shows that β can be easily calculated with inputs of the simulator, including compressibility, oil viscosity, fracture half-length, etc. Third, the previous section has derived the combined productivity index model equation based on the analytical solution to the linear transient flow regime and the constant productivity index behavior during semi-steady state flow regime. The production history including both the above flow regimes can be fitted simultaneously to Equation 8 with β as a fitting parameter. Every model fitting with simulations of various permeability values will produce a corresponding β value that can be used to correlate with permeability inputs.

By performing the above calculation and model fitting, a correlation between β and the square root of permeability is shown in Figure 28. All three methods show very strong linear correlations between the two parameters with correlation coefficient above 0.9. The correlations derived from production history in only linear transient regime and the one calculated from simulator all extrapolate to the origin, indicating that when the permeability is zero and corresponding β value is also zero. However, the correlation derived using the entire production history does not extrapolate to zero. The possible reason is that, as shown in Equation 8, the analytical solution to the linear transient flow regime is revised to fit the production history better by not restricting n component to -0.5. Such revision to some extent compromises the accuracy of the prediction of the fitting parameters for linear transient regime, leading to the non-zero intercept in Figure 28.

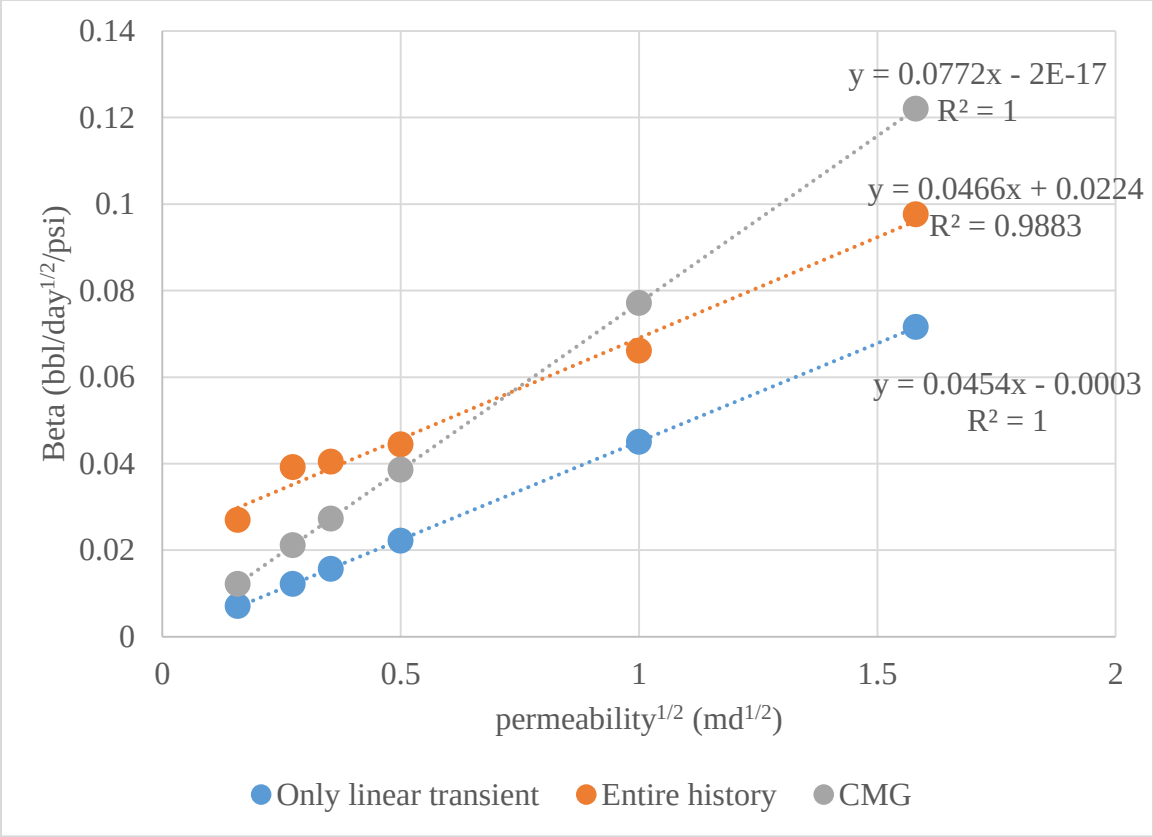

Figure 28: Correlation between beta and square root of permeability with three different methods

The definition of β shows that it is proportional to the square root of permeability. In other words, the log-log plot of β vs. permeability should show a one-half slope. Such a log-log plot with β calculated from three different methods is shown in Figure 29. Two black lines are lines with one-half slope. The figure shows that β calculated with only production history within the linear transient flow regime and that from simulator show a one-half behavior as predicted while β calculated using the entire history does not. This abnormality is also because of the compromises made to fit the production history by altering the exponent of time. However, the proposed model is still

valid even with certain degree of compromises and can capture the behavior of the productivity index in two different regimes

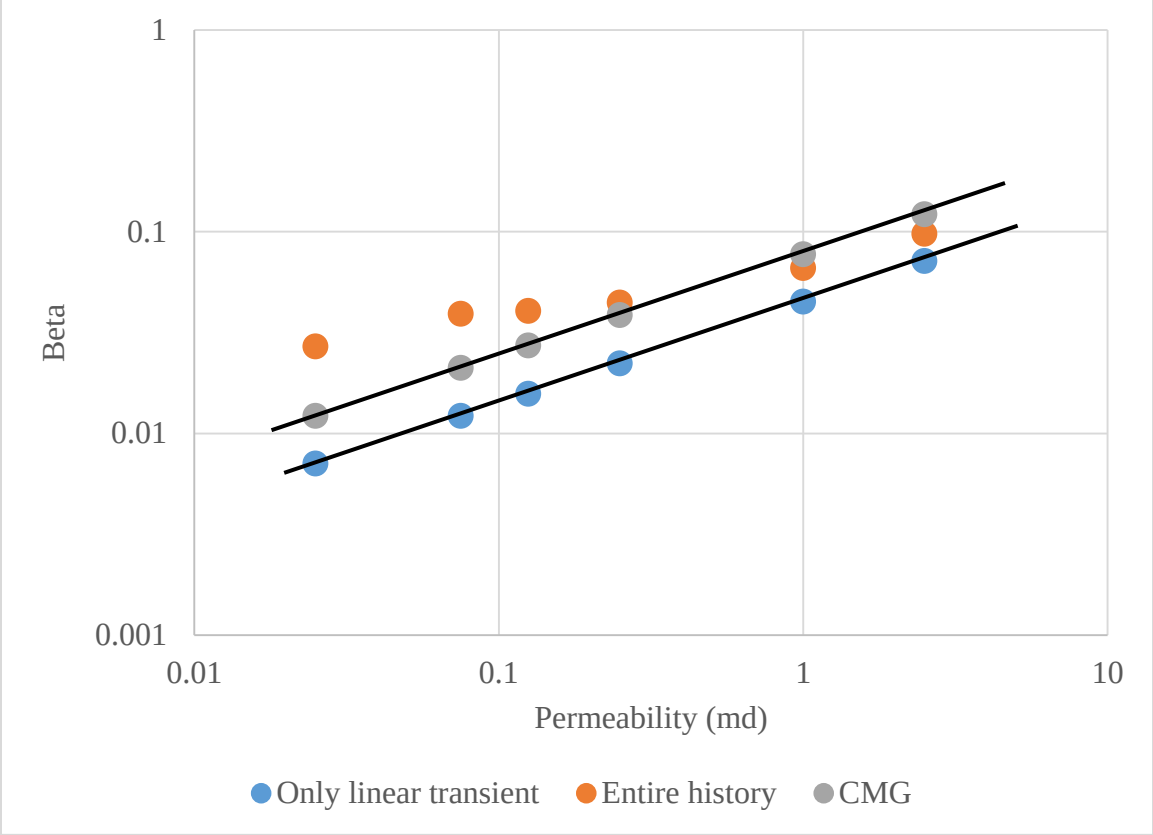

Figure 29: Log-log plot of β vs. permeability

COMBINED CRM MODEL SENSITIVITIES TO FITTING PARAMETERS

It is important to examine how different values of fitting parameters in the combined CRM model affect the production behavior, and such analysis will assist in understanding how this model reflects the physics of fluid flow in both linear transient and semi-steady state flow regime.

Equation 11 offers the opportunity to calculate the flow rate at each time step with given fluid and reservoir properties, such as compressibility, viscosity, etc. The default values for steady state productivity index is 2×10^{-2} bbl/day/psi, β is 1.22×10^{-1},

$c_t V_p$ is 6.42 and n is 0.7. This set of parameters come from the model fitting to the simulated production history with permeability of 2.5 md, as shown in Table 4. Figure 30 shows the effect of various steady state productivity index on the flow behavior. While keeping all other parameters the same, three logarithmically spaced steady state productivity index values are chosen ranging from 1×10^{-4} to 1×10^{-2}. The range is chosen based on various fitting results from the previous chapter.

As emphasized in the previous section, the steady state productivity index is a characteristic of the steady state flow regime. The larger the value, the more dominant the steady state regime is as shown in the Equation 7. In an extreme case, if the steady state productivity index, which is the second term in Equation 7, then the effect of the first term representing the linear transient regime is completely negligible. In that case, the combined productivity index will be independent of time, and the production behavior will be an exponential decline from the very beginning. On Figure 28, the production performance when J is 1×10^{-2} bbl/day/psi is clearly an exponential decline for the most part. When the productivity indices become smaller, as represented in the red and green curves, the steady-state flow regime almost disappears and the entire history is in a transient regime, because the linear transient term regains the dominance.

Figure 31 demonstrates the effect of β on the production history. Contrary to the effect of steady-state productivity index, the larger β value, the more significant the linear transient regime. As shown in Figure 31, the blue curve shows a longer transient regime than the red and green curves, simply because the β value of the blue curve is bigger.

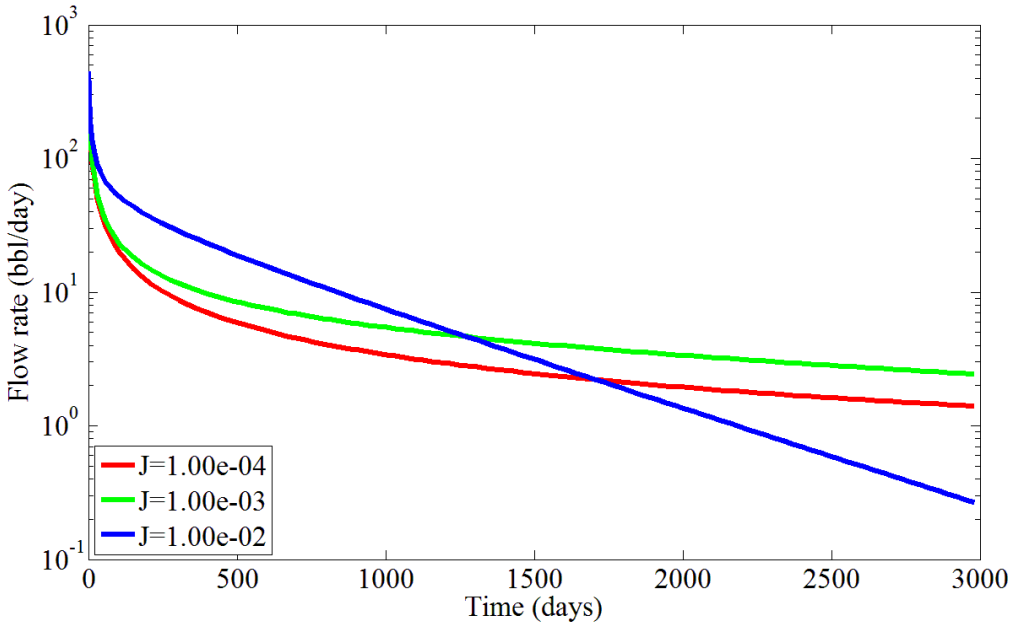

Figure 30: Production history with various steady state productivity indices

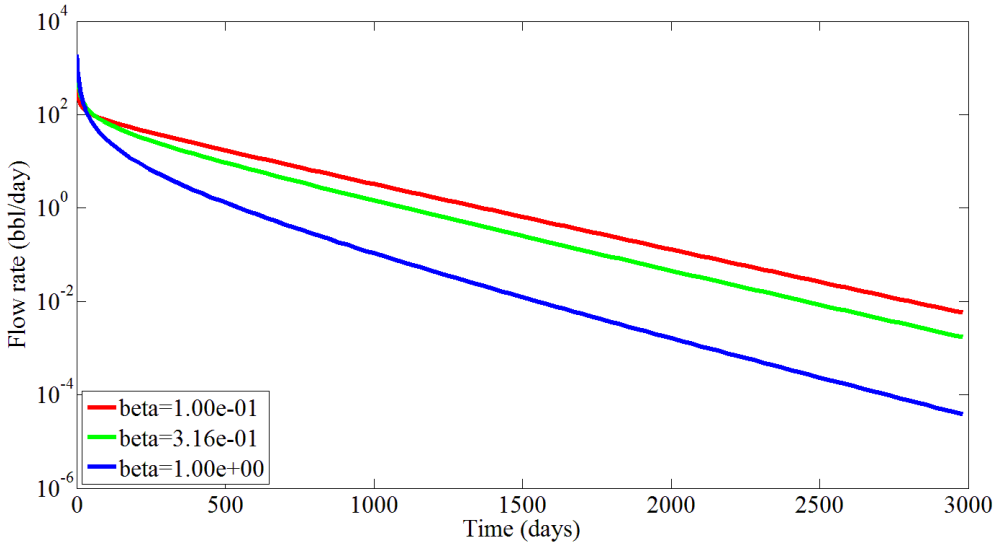

Figure 31: Production history with various beta values

COMBINED CRM TO MATCH FIELD PRODUCTION HISTORY DATA

After obtaining good matches with synthetic cases, the next goal is to test whether the combined CRM is able to match field data. Figure 32 is the field production data from well 74 drilled in the middle Bakken formation. The first production is reported on 08/09/2007, and all production rates were reported daily. The latest production was reported on 09/12/2010. The production profile has some oscillations, but overall the production is relatively smooth. The initial production is very large at about 400 bbl/day, and declines dramatically after the first 18 months to about 75 bbl/day, and then the production reaches a very gradual decline with relatively small production rate.

The combined CRM is fitted to the field data, shown in Figure 33. The model is able to fit the fast decline at very early stage of the production as well as the long period of low production rate later on. The errors between the field data and the modeled data are plotted in a histogram shown in Figure 34. The error residuals observe an approximately normal distribution with a mean of -0.06 bbl/day and a standard deviation of 33 bbl/day. There are a couple of points that are almost 10 times bigger than the standard deviation, including the very first modeled data point that is 800 bbl/day bigger than the actual data. The rest of the error residuals appear to be well captured by the normal distribution.

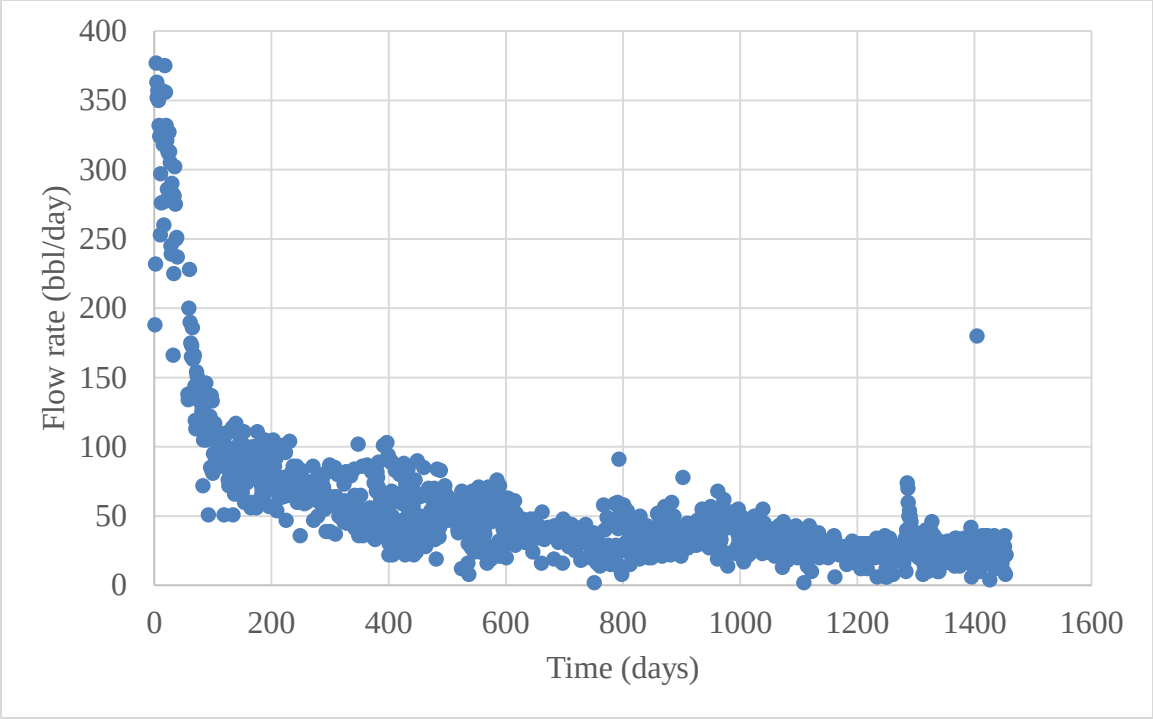

Figure 32: Production history for well 74 in the middle Bakken formation

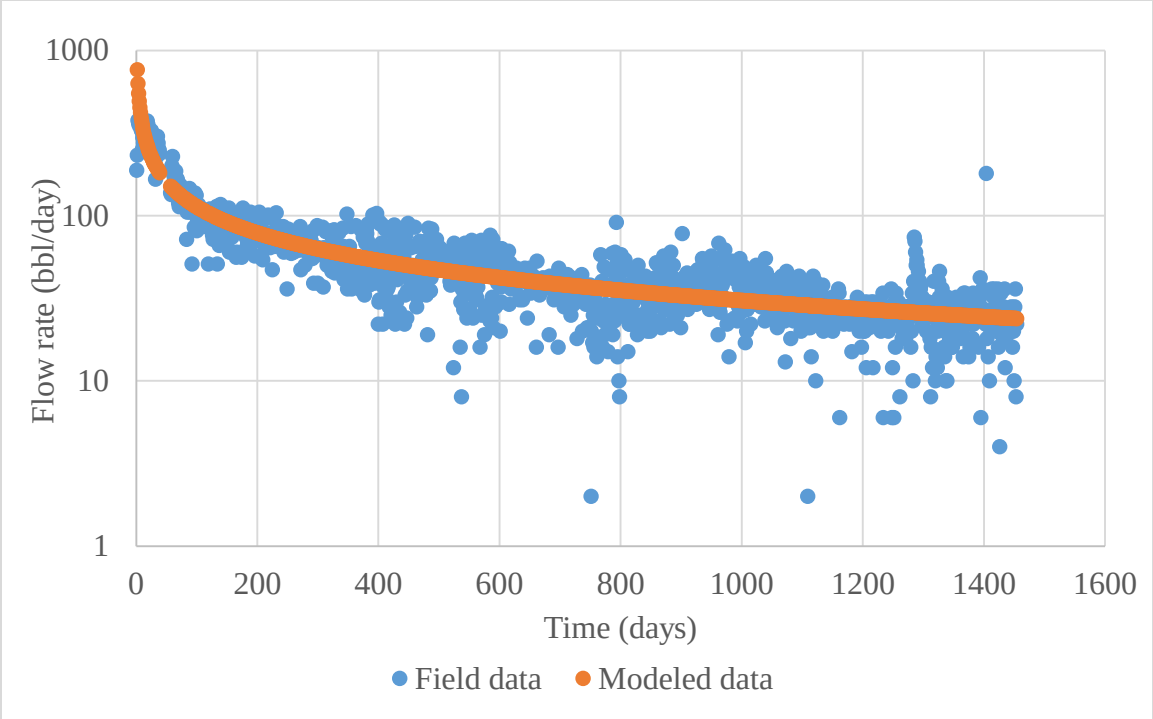

Figure 33: Combined CRM fit to field data from well 74 in middle Bakken formation

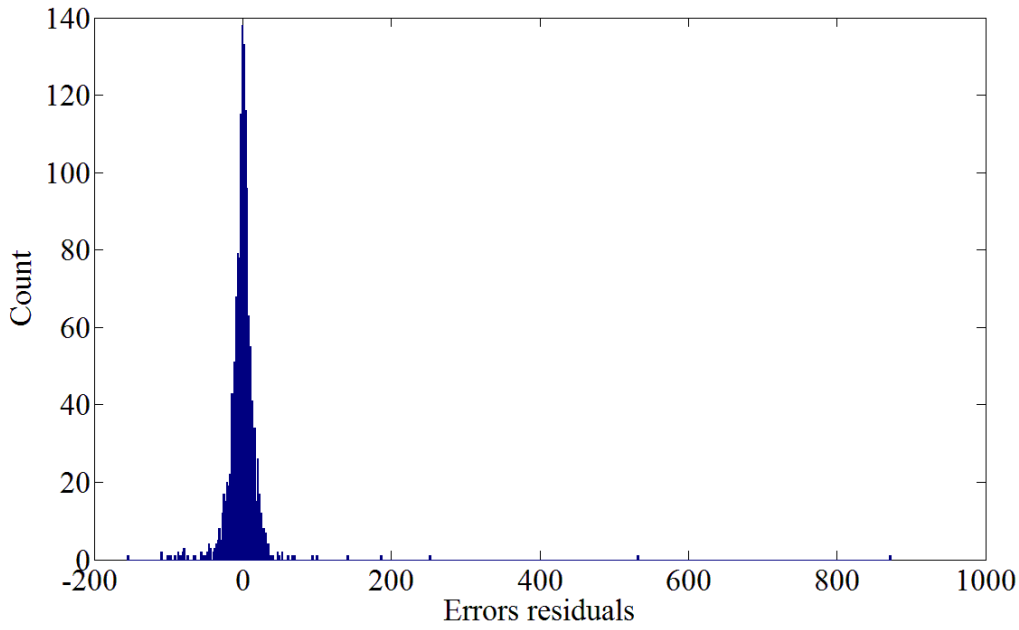

Figure 34: Error residuals between the field data and modeled production data

Since the combined CRM is a physics-based reservoir model, the total ultimate production predicted by the model should be physically viable, which means that the daily production rate should reach 0 bbl/day. By extrapolating the existing production history to infinity, the production rate should reach 0 bbl/day and thus the cumulative production should yield a EUR. Figure 35 shows that the production forecast will reach 0.01 bbl/day at about 100,000 days. Hence, the model prediction is more realistic than the logistic CRM, which never reaches zero flow rate.

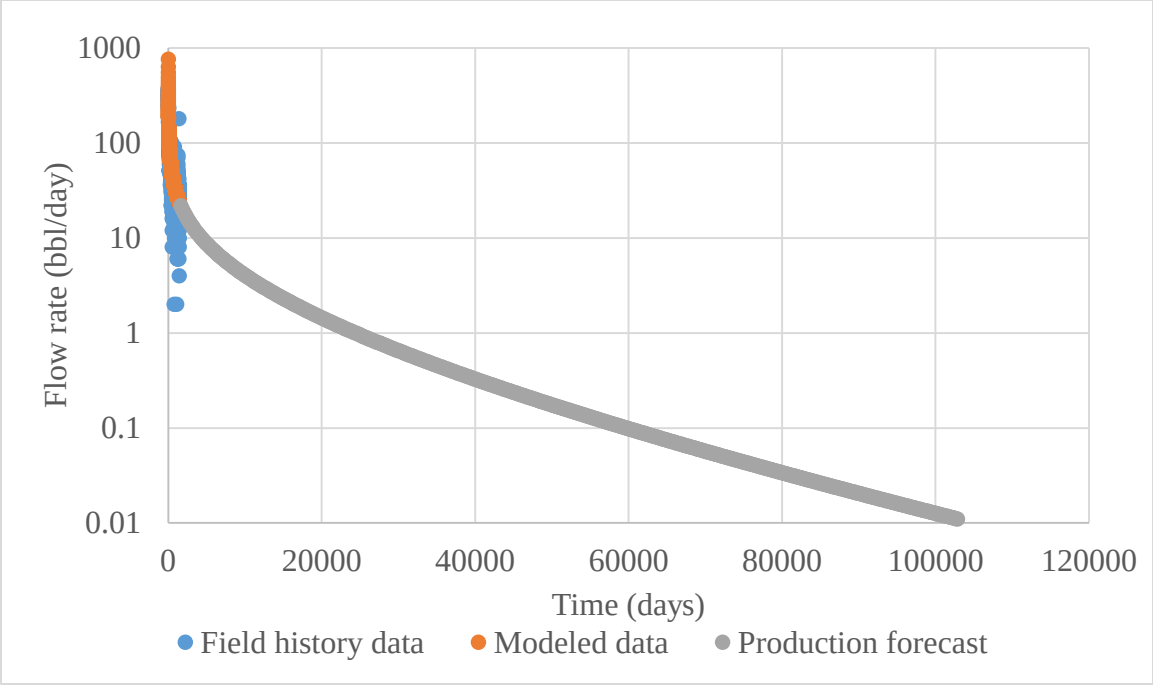

Figure 35: Production forecast with combined CRM based on fitted data

Chapter 4: Logistic CRM Formulation

ORIGINS OF LOGISTIC GROWTH MODELS

The logistic growth models are a family of mathematical models developed for a wide range of fields, including biology, economics, statistics, etc. The model was first proposed to model the restricted population growth.

Based on the rational that the population in the world cannot expand infinitely and that there must be a limit to the population growth, Verhulst developed the logistic growth model in 1838 to represent that the size of human population has a limitation, referred to as the carrying capacity (Verhulst 1838). The logistic model is built upon the exponential grow model, which has a fundamental equation:

$$\frac{dN}{dt} = rN \tag{14}$$

Where

N = Population

r = Constant

t = Time

This rate-time relationship can be integrated with initial population N_0 to obtain the population-time relationship:

$$N = N_0 e^{rt} \tag{15}$$

Where

N_0 = Initial population

Such model describes an infinitely increasing behavior as shown in Figure 36, which according to Malthus was unrealistic (Malthus 1872).

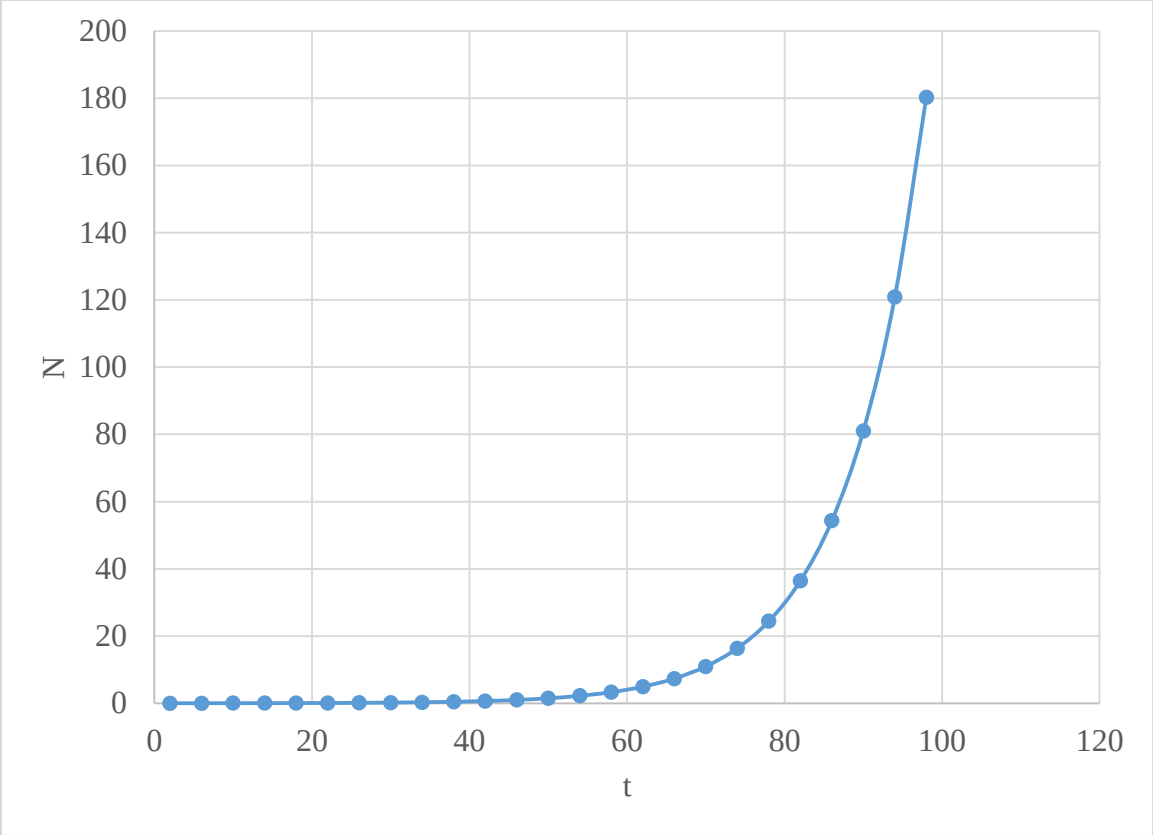

Figure 36: Population (N) vs. time (t) in an exponential model

The rationale behind Malthus's philosophy is that the natural resources are limited, so the population could not grow without an upper limit. Verhulst (Verhulst 1838) adds a multiplicative factor to Equation 14 to curtail the unbounded population growth.

$$\frac{dN}{dt} = rN\left(1 - \frac{N}{K}\right) \tag{16}$$

The equation can be integrated to obtain the cumulative population over time.

$$N = \frac{K}{\left(\frac{K}{N_0} - 1\right)e^{-rt} + 1} \tag{17}$$

The carrying capacity, K, limits the rate at which the population grows. In Equation 16, the left side is the rate of population growth. The population growth starts

from zero, forcing the right side of the equation to be identical to the exponential model. So the population grows in an exponential manner at the beginning. As the population N approaches the carrying capacity K, the right side of the equation will approach zero. Thus, the population stops growing, and the population reaches a certain level. Because of the nature of the Verhulst logistic growth equation, the model shows a characteristic S-shape, as shown in Figure 37.

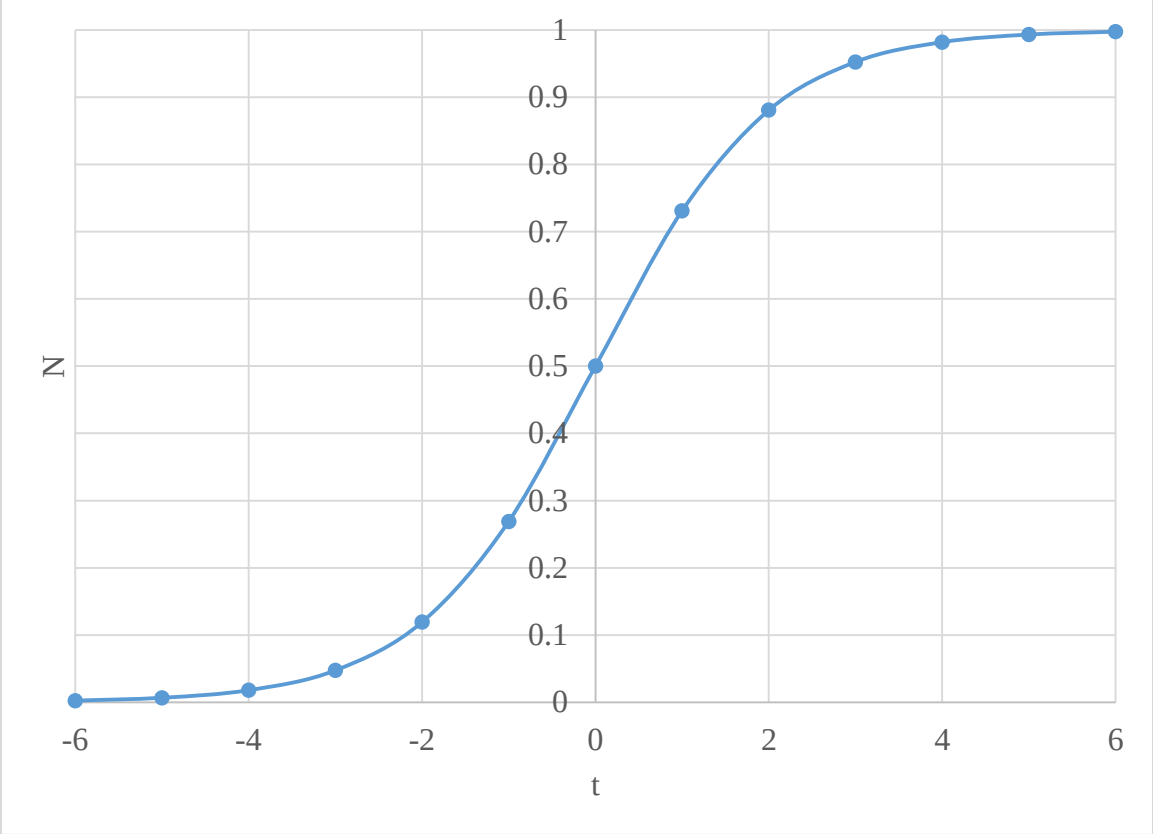

Figure 37: Standard logistic sigmoid function

PROPOSAL OF LOGISTIC PRODUCTIVITY INDEX MODEL

The classic productivity index equation (Equation 1) shows that the flow rate is proportional to the difference between average reservoir pressure and well bottom hole pressure if the productivity index remains constant. In fact, under semi-steady state flow

regime, the productivity index is a constant, and thus in this flow regime the flow rate varies linearly with the change in the pressure difference (Walsh and Lake, 2003).

To formulate a productivity index model suitable for transient flow, it is important to mathematically describe the relationship between flow rate and drawdown pressure in linear transient and semi-steady state flow regime collectively. To propose such a relationship, pressure difference versus flow rate results from single compartment model simulation were run with permeabilities of 0.025, 0.075, 0.25, and 2.5 md. Figure 38 shows the results.

As demonstrated in the last chapter, the production history with permeability of 0.025 md is entirely in the linear transient flow regime while that with permeability of 2.5 md has significant amount of time in both the linear transient and semi-steady state flow regimes. Histories with permeabilites of 0.075 and 0.25 md have relatively more linear transient regime data. The pressure difference versus flow rate plot does not have an explicit time scale, which instead is implicitly expressed in the flow rate.

The declining nature of the well performance in Figure 38 is manifested in the flow rate, the production starts from the top right corner where the flow rate is the highest and gradually declines to smaller production at the bottom left corner. As demonstrated in the last chapter, when the permeability is 0.025 md, the entire production history is in the linear transient regime while the majority of production history is in the semi-steady state flow when the permeability is 2.5 md. In the pressure drawdown vs. flow rate plot, the plot only has the upper right portion in the 0.025md case and the 2.5 md plot has extended period at the bottom left corner with very little upper right corner. This is showing that the top right portion represents the linear transient flow regime and the bottom left semi-steady state flow regime. If the pressure propagation has not reached the

pressure boundary as in the permeability of 0.025 md case, there will not be bottom left portion.

It is a common practice to plot production rate on a log scale, and in the presence of both linear transient and semi-steady flow, the semi-log plot yields an S-shaped profile. In comparison, with data within linear transient flow regime, only a portion of S-shaped profile is present. The S-shaped pressure difference versus flow rate matches with the classic profile of logistic growth model really well, so it is proposed to model the relationship between these two parameters with the logistic growth model, which takes the form of:

$$Y(X) = \frac{L}{(C + Qe^{-BX})^{\frac{1}{v}}} \tag{18}$$

Where C, Q, B, and v are model parameters. Based on this general mathematical form, the relationship between pressure drawdown and oil rate obeys the following model:

$$\bar{P} - P_{wf} = \frac{L}{(C + Qq^{-B})^{\frac{1}{v}}} \tag{19}$$

The log of oil rate is used to preserve the S-shaped behavior that is observed when oil rate is plotted on a log scale. In comparison to combined productivity model, which is proposed based on the analytical solution of respective flow regimes, logistic productivity index model does not make the distinctions on flow regime, and regard the entire production history as a whole package.

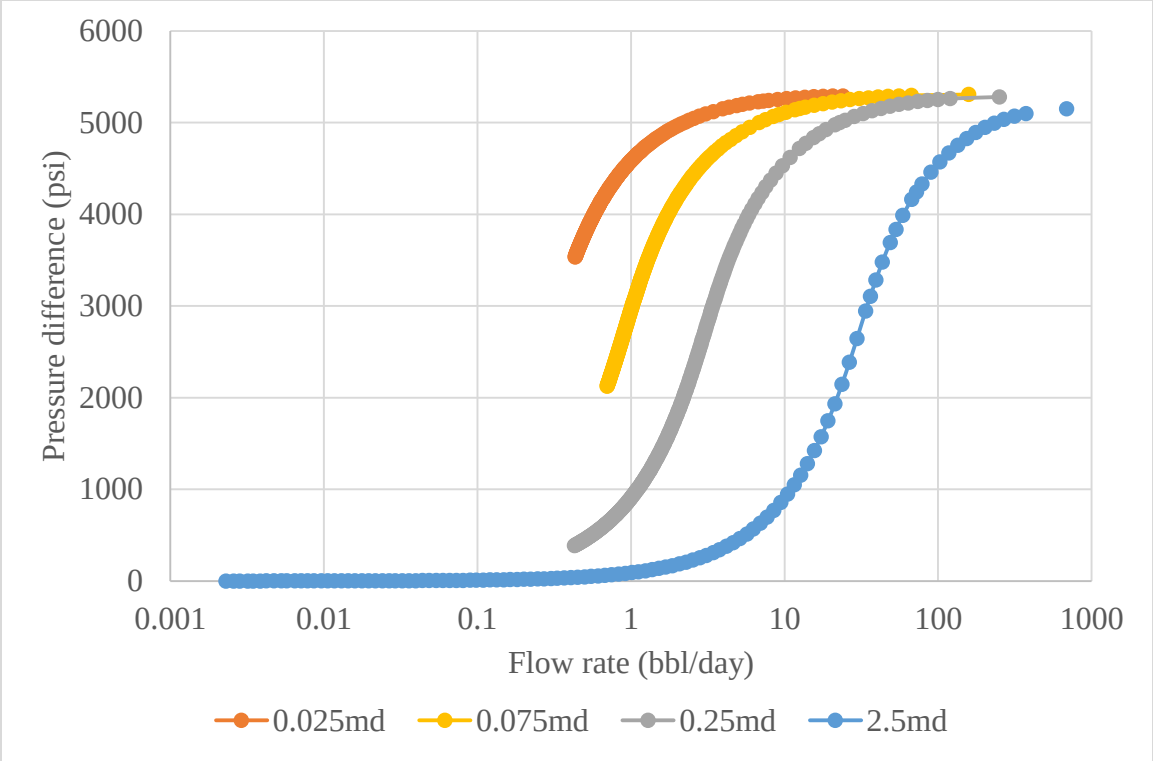

Figure 38: Simulation results of pressure difference vs. oil rate for various permeabilites

VALIDATION OF LOGISTIC PRODUCTIVITY INDEX MODEL

The validation of the model is done with Microsoft Excel Solver. The historical ln(q) and pressure difference come from the single-compartment model simulation. From the proposed model in Equation 19, the modeled pressure difference can be calculated for each ln(q) given a set of initial guesses for model parameters L, C, Q, B, and v. Then solver is used to minimize the sum of squared errors between the simulations results and the modeled values. Two typical cases are in Figures 39 and 40 with permeability of 0.025 and 0.25 md, respectively. The logistic growth model is able to match the relationship between ln(q) and pressure difference very well with minimal errors. The errors for both cases are generally under 5%, and the biggest differences appear at around the inflection points. Table 5 and 6 shows the fitting parameters of these two matches.

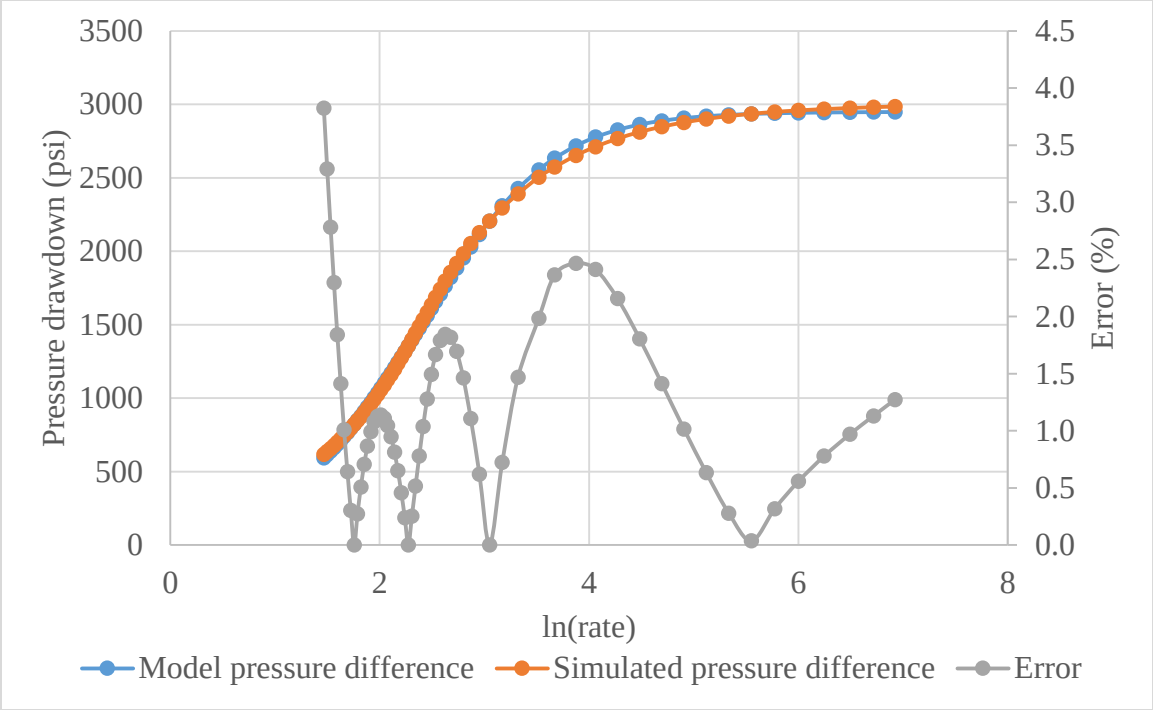

Figure 39: Model match of pressure difference versus rate (0.025 md)

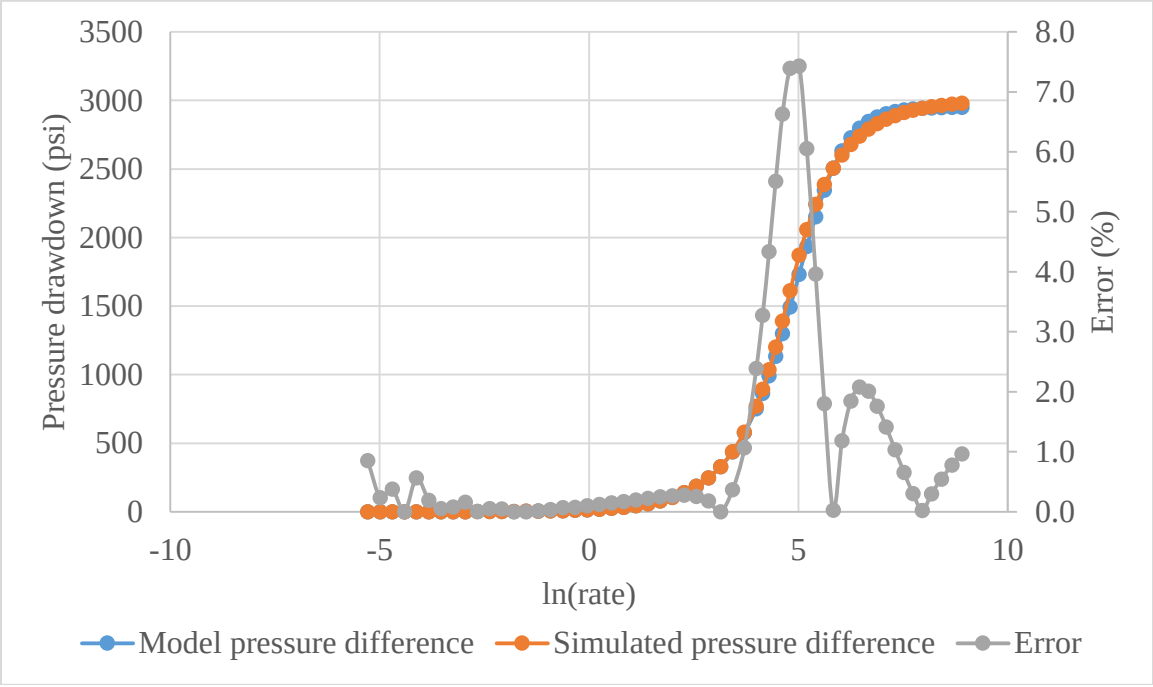

Figure 40: Model match of pressure difference versus rate (0.25 md)

Fitting parameters	Value
L	724.4
C	0.1
Q	2012.5
B	1.9
v	1.9

Table 5: Fitting parameters for the model match in the case of 0.25 md

Fitting parameters	Value
L	1602.6
C	0.5
Q	37.7
B	1.7
v	1.3

Table 6: Fitting parameters for the model match in the case of 0.025 md

LOGISTIC CRM TO MATCH HISTORY DATA

After validating that the logistic growth model is able to describe the relationship between drawdown pressure and flow rate, the model can be then incorporated into the material balance equation of CRM to eliminate the pressure so that a model involving flow rate and time can be derived.

By rearranging the logistic productivity index equation (Equation 15) and inserting into the fundamental CRM equation (Equation 9), we obtain (details in Appendix B)

$$q_{n+1} = -q_n^{B+2}(C + Qq_n^{-B})^{\frac{v^2+1}{v}} \frac{v\Delta t}{c_t V_p LQB} + q_n \tag{20}$$

The semi-analytical solution is obtained by explicit finite difference, since the above equation cannot be solved analytically. In this solution, q_n is the flow rate from last time step, and q_{n+1} is the flow rate at the current time step. Δt is the time difference between the last and the current time step.

To validate the logistic CRM, a history match is also achieved with Microsoft Solver. Figure 41 shows the history match for permeability of 0.25 md by using Solver on a log-log scale and the percentage of errors between the simulation and the model. The match during linear transient regime is really good, and the errors are generally below 6%. On a log-log scale, it is difficult to observe the quality of the match after fracture interference, so Figure 42 shows the fitting quality on a semi-log scale. From the plot, it can be seen that the general fitting quality is still decent. Overall, the logistic CRM can fit both linear transient and facture-dominated regime reasonably well.

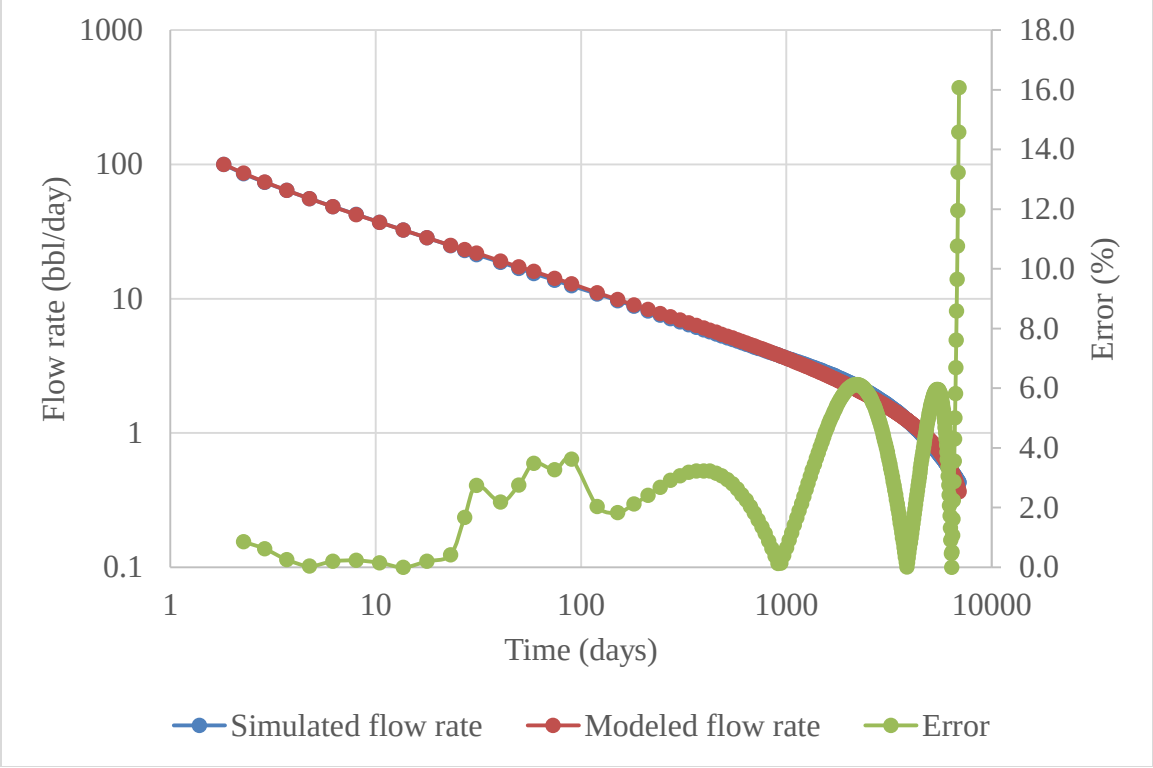

Figure 41: History match of logistic CRM on log-log scale (0.25 md)

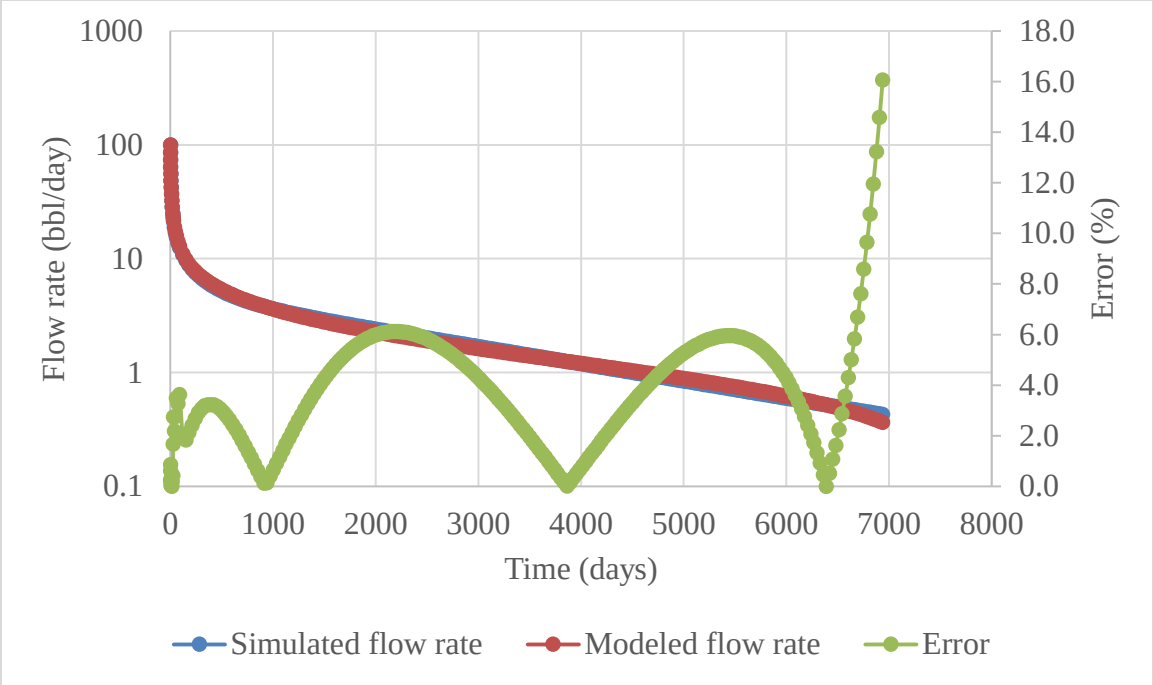

Figure 42: History match of logistic CRM on semi-log scale (0.25 md)

The field data of well 74 is also used to validate the application of such model to realistic production data. Figure 43 plots the field production history and two types of model fit with both logistic and combined CRM model. The fitting qualities of both models are almost identical for the majority of the production history, but the logistic model can further reduce the model errors at the very early stage. The error for the first data point is only 245 bbl/day in comparison to 800 bbl/day error by using combined CRM. The error residuals histogram is shown on Figure 44, which has a mean of -1.33 and a standard deviation of 18. Undoubtedly, the logistic CRM provides better fitting to the field data. However, because the model is not physics-based, the model does not extrapolate to zero flow rate as shown in Figure 45 and thus leads to infinite oil production.

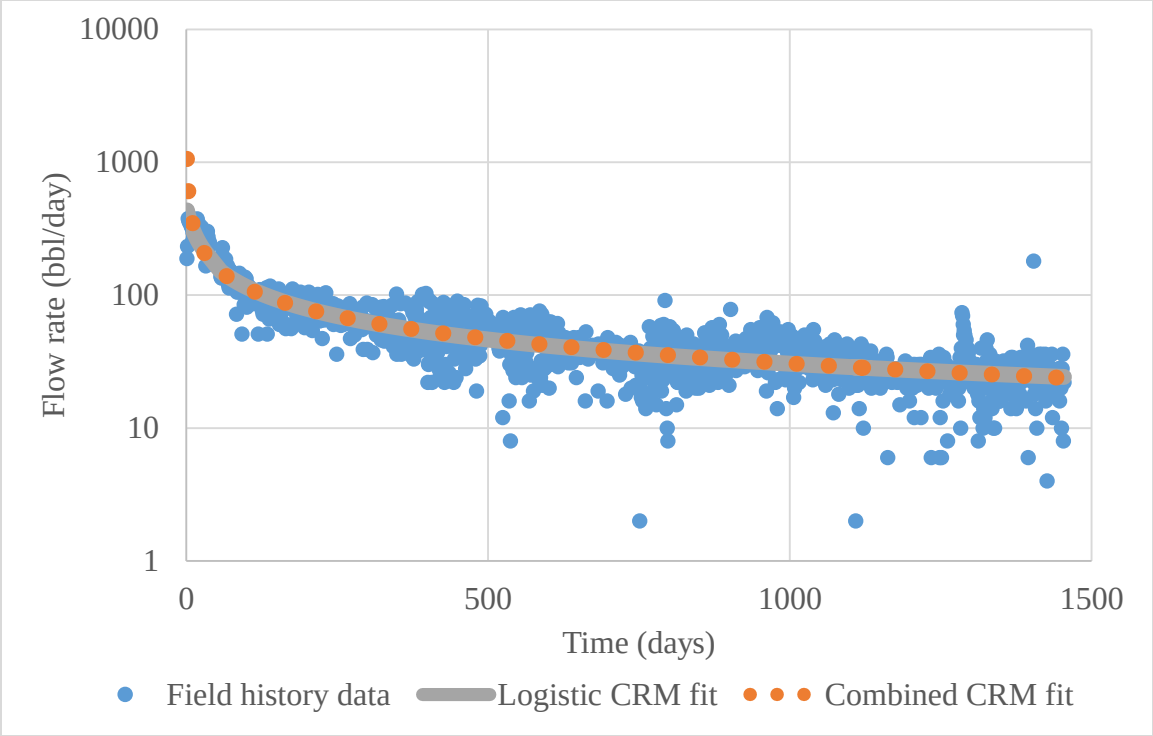

Figure 43: Model fit comparison with logistic and combined CRM with field data

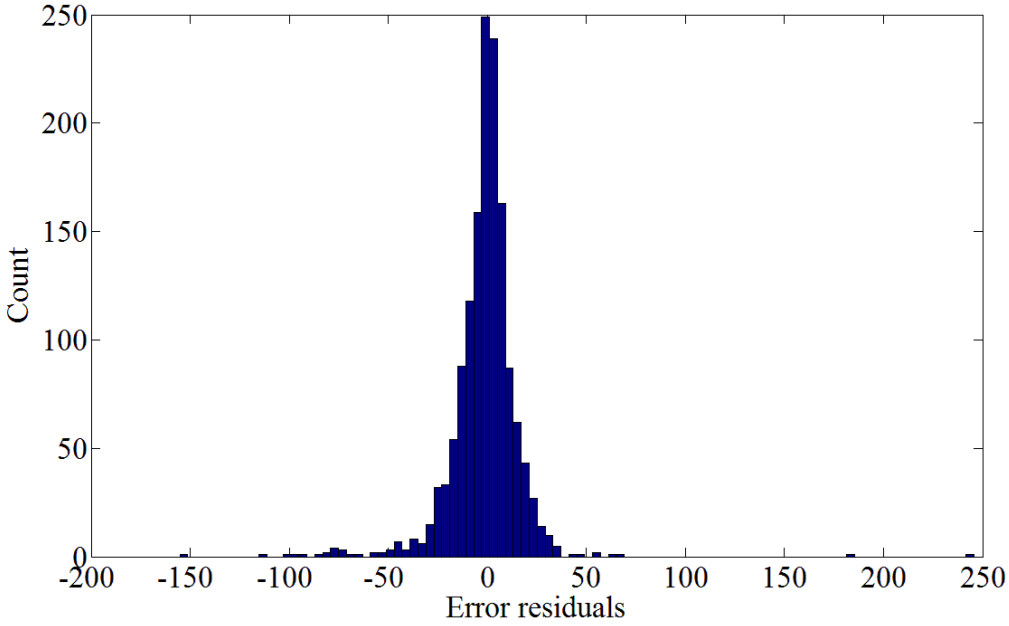

Figure 44: Error residuals for logistic CRM model fit

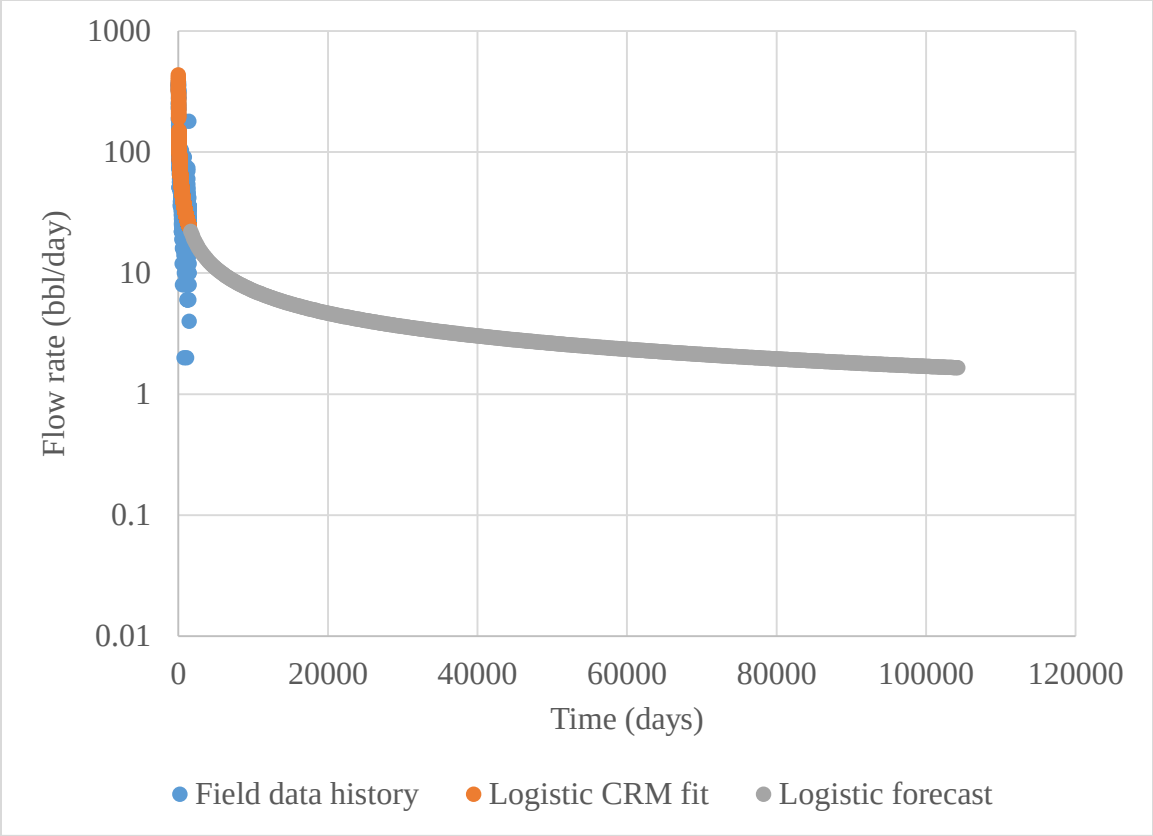

Figure 45: Production forecast with logistic CRM

From the above analysis, logistic CRM provides the best data fitting quality; however, it leads to unphysical results. The model fitting with combined CRM is slightly inferior, but its model predication yields a EUR after extrapolation. In conclusion, the combined CRM model is the more reliable model of the two to history match and predict future oil production.

Chapter 5: Non-uniqueness of History Match

As Appendix A and B show that the solution to the combined and logistic CRM are extremely non-linear, with multiple terms multiplied together of which some are even at the exponent. In such a system, the solutions obtained from a single optimization might not be unique. In this chapter, the non-uniqueness of history match with various objective functions and initial guesses is investigated.

NON-UNIQUENESS RESULTING FROM OBJECTIVE FUNCTIONS

To achieve a history match with either combined or logistic CRM model, an objective function must be used to minimize the errors between the simulated production data (SPD) and the modeled production data (MPD). The quality and the fitness of the selected objectives functions will significantly impact the quality of the history match. There are three different objective functions experimented in the above history matches, and they are:

$$Objective\ function\ 1: error = absolute\ value\ of\ (SPD - MPD) \quad (21)$$

$$Objective\ function\ 2: error = absolute\ value\ of\ (SPD^{\frac{1}{2}} - MPD^{\frac{1}{2}}) \quad (22)$$

$$Objective\ function\ 3: error = absolute\ value\ of\ (\ln(SPD) - \ln(MPD)) \quad (23)$$

All three objective functions are used to history match the same simulation results run with 2.5 md permeability to analyze the sensitivity of fitting qualities to objective functions. The same results are shown on semilog and log-log scale respectively in Figure 46 and 47. In Figure 46, different objective functions lead to dramatically different behaviors during the exponential decline. The dark blue curve is computed using objective function 3, and is completely overlying on the simulated production data and matching the exponential decline portion of history data perfectly. The orange curve is computed using objective function 2, and matches with the simulated production data

very well until about 1500 days when the modeled production data starts to deviate. The worst match of all three objective functions is function 1; the majority of the curve is not able to match the simulated production data

In contrast, Figure 47 shows that there are very subtle differences between using different objective functions to match the simulated production history during the linear transient flow regime, and the history match with function 1 is the best.

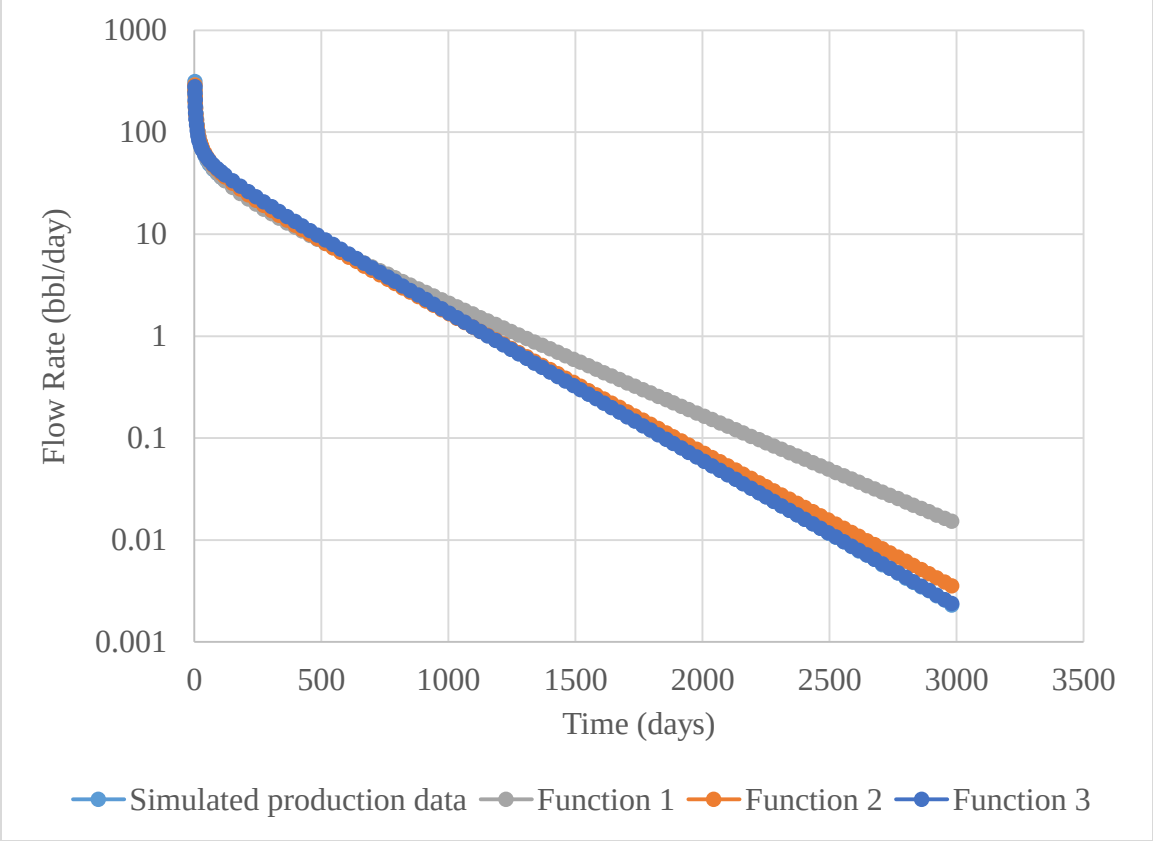

Figure 46: Simulated production data (2.5 md) history match with three different objective functions on log-log scale

The reason behind such phenomenon is that the production history of a single compartment model has a unique characteristic. At the start of the linear transient flow regime, the production rate is very high, then it declines very fast and reaches a low rate

during the semi-steady state flow regime. For example, in Figure 46 and 47, the initial production rate is about 300 bbl/day, but at the end of the production the rate is almost 0.002 bbl/day. These two rates are off by five orders of magnitude. The result is that the errors between simulated and modeled production history are trivial during semi-steady state regime because of their absolute magnitude while the errors during linear transient regime are more pronounced, so if only the absolute values of the differences are taken into account, the model will fit the early stage production data by compromising the fitting quality of the later stage.

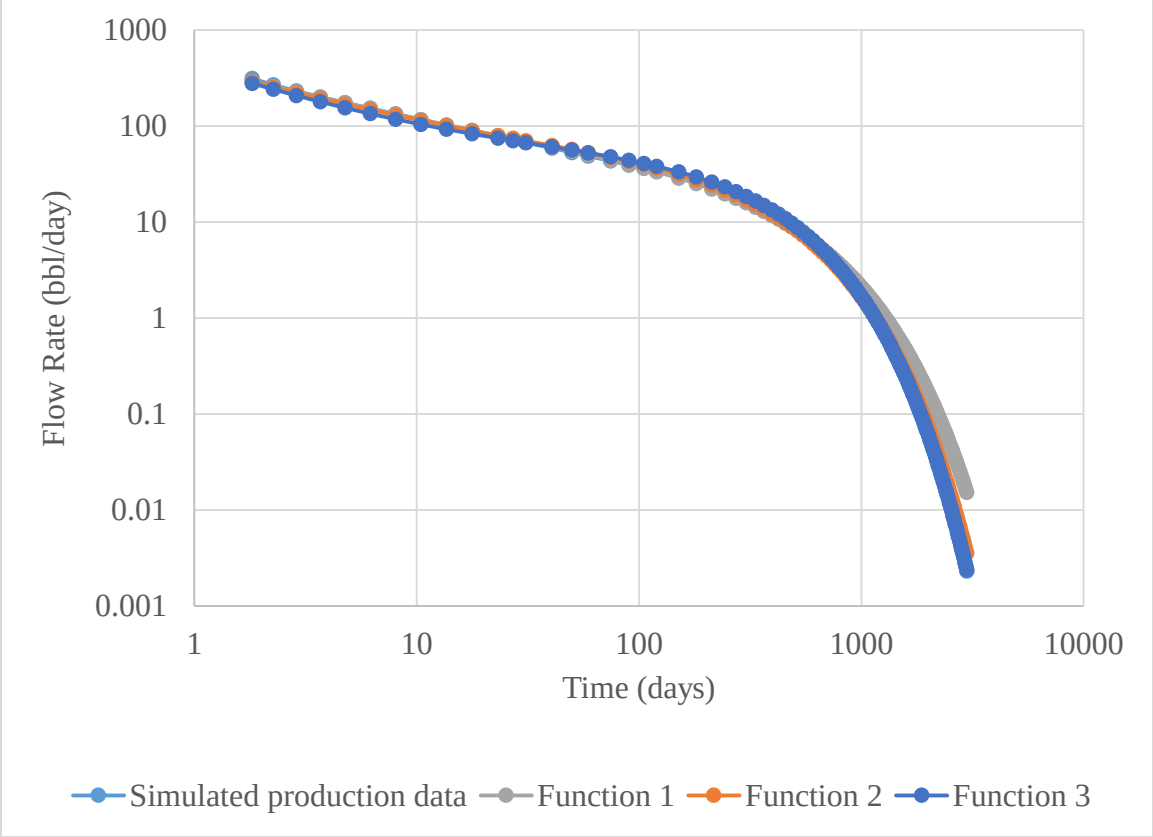

Figure 47: Simulated production data (2.5 md) history match with three different objective functions on log-log scale

In comparison, taking a one-half power and logarithmic function to both simulated and modeled production data will significantly reduce the magnitude of the early time production data, and thus prevent the errors at the early stage dominating the sum of errors calculation. This enables the objective functions to minimize the errors for the entire production history. Figure 46 and 47 show that taking the logarithmic function to the data will offer the best fitting for the overall simulated production history, which is used as the objective functions for all the history match presented in previous chapters.

NON-UNIQUENESS RESULTING FROM INITIAL GUESSES

To initiate the optimization of curve-fitting, a set of initial guesses for model parameters is required. If the solution is unique, similar parameter inputs will converge to the exact same modeled parameters. However, in the case of combined CRM model-fitting, because of the non-linearity of the model, various initial inputs can lead to different optimized results. Figure 48 shows how different initial guesses change the fitting results. After obtaining a set of fitting results, shown as the Original Results, the beta is changed from 4.4×10^{-2} to 6×10^{-2} bbl/day$^{1/2}$/psi and the optimization is conducted in Solver with a new beta value. With only a small change in the beta parameter, the optimized results are quite different as shown in Guess 1. All four parameters have changed their values with the sum of errors remain the same. Then the beta value is changed from 5.12×10^{-2} to 3×10^{-2} bbl/day$^{1/2}$/psi to run another optimization, the fitting parameters change again.

Comparing the fitting parameters from Guess 1 to those from Guess 2, the changes in n is trivial; however, the changes in other three parameters exceed 16%. The Figure 48 shows the simulated and modeled production history with the original initial guesses and two different initial beta guesses. The blue curve indicates the simulated

production history. The rest of the curves collapse into one curve and only one of them is visible on the figure, showing that different fitting parameters can lead to nearly identical graphical results. The non-unique optimization will result in inconsistent parameters predictions with combined CRM model. Similarly, the non-uniqueness is also present in the logistic CRM model.

	Original Results	Guess 1	Guess 2
J	1.47E-03	1.70E-03	1.41E-03
beta	4.44E-02	5.12E-02	4.27E-02
n	-6.68E-01	-6.69E-01	-6.69E-01
ctvp	5.03E+00	5.80E+00	4.82E+00
sum of errors	5.76E+00	5.76E+00	5.76E+00

Table 7: Fitting results with various initial guesses

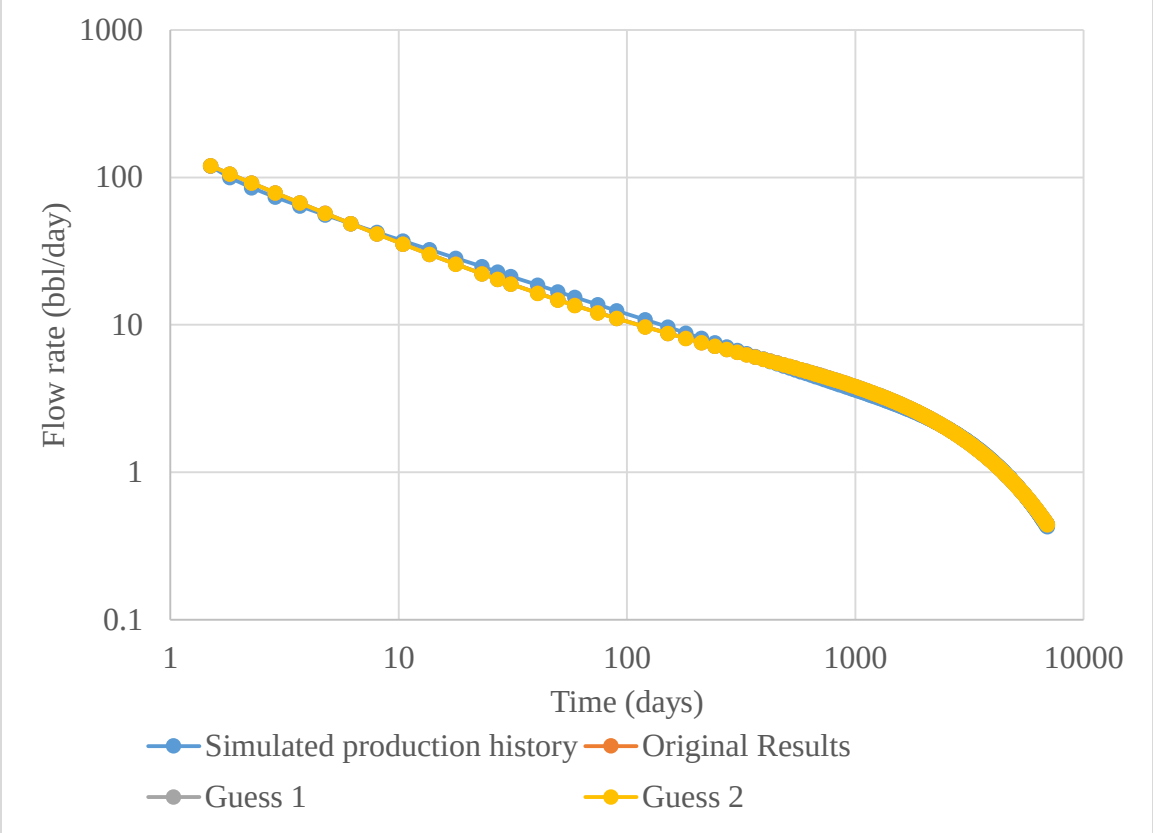

Figure 48: Simulated and modeled production history with various initial guesses

Chapter 6: Conclusions and Future Works

CONCLUSIONS

The reservoir model, if built carefully, is able to simulate both linear transient flow and fracture-dominated flow behavior as derived in Wattenbarger and El-Banbi's analytical solution to the single compartment model. Based on their early stage approximation of the linear transient solution and the constant productivity index during fracture-dominated flow, a combined productivity index equation is proposed. This equation establishes a closed relationship between flow rate and time so that it can be incorporated into the material balance equation for CRM to derive average pressure as a function of time. Such a model can match the production history from single compartment model simulation really well. This model is physics-based, so the fitting parameters are also important reservoir properties. The fitting results from multiple simulations show that the more data there is for a specific flow regime, the more accurate the prediction for the characteristic parameter in that regime.

It is also shown that the relationship between pressure difference and natural log of flow rate shows an S-shaped profile that can be modeled with a logistic growth model. The logistic growth model can also fit the simulation data very well. This model establishes a closed relationship between pressure and time. Such a relationship eliminates the flow rate dependency in the fundamental CRM equation so that flow rate as a function a time can be derived. The resulting model can fit synthetic as well as field data with high accuracy.

FUTURE WORKS

1. Investigate the sinusoidal behavior in the combined CRM, and further improve its accuracy

2. The combined model suffers from certain degree of mismatch during the transition period from linear transient to fracture-dominated flow regime. It might be because of the simplicity of the linear combination of two components in the model. It would be worthwhile to investigate a better way to connect the productivity index for linear transient and the constant productivity index region.
3. Reservoir simulations with more realistic reservoir and fluid property parameters are necessary to further justify the applicability of the proposed models in realistic field cases.
4. Adopt the same methodology for transient CRM applications in radial flow geometry.
5. Optimize the model to reduce the non-uniqueness resulting from various objective functions and initial guesses.

Nomenclature

B: $Formation\ volume\ factor$ $[bbl/STB]$

β: $Parameter\ in\ combined\ CRM\ model$ [bbl/day$^{1/2}$/psi]

c_t: $Total\ compressibility$ $[psi^{-1}]$

C: $Parameter\ in\ logistic\ growth\ model$

$DTMAX$: $Maximum\ time\ step\ in\ CMG\ IMEX$

h: $Fracture\ height$ $[ft]$

K: $Carrying\ capacity\ in\ logistic\ grow\ model$

k: $Permeability$ $[md]$

L: $Parameter\ in\ logistic\ growth\ model$

J_∞: $Steady-state\ productivity\ index$ $[bbl/day/psi]$

J: $Productivity\ index$ $[bbl/day/psi]$

μ: $Viscosity$ $[cp]$

P_i: $Initial\ reservoir\ pressure$ $[psi]$

n: $Parameter\ in\ combined\ CRM\ model$

N: $Cumulatvie\ production$ $[bbl]$

ϕ: $Porosity$ [%]

P_{wf}: $Flowing\ bottom\ hole\ pressure$ $[psi]$

$\bar{P}$: $Average\ reservoir\ pressure$ $[psi]$

Q: $Parameter\ in\ logistic\ growth\ model$

q: $Flow\ rate$ $[bbl/day]$

q_D: $Dimensionless\ flow\ rate$

r: $Parameter\ in\ logistic\ growth\ model$

t: $Time$ $[day]$

t_{Dxf}: $Dimensionless\ time$

τ: $Time\ constant, equilavent\ to \frac{c_t V_p}{J}$ $[day]$

v: $Parameter\ in\ logistic\ growth\ model$

V_p: $Pore\ volume$ $[ft^3]$

x_f: $fracture\ half\ length$ $[ft]$

Appendix A: Derivations of Combined CRM

Material balance equation for CRM:

$$V_p c_t \frac{d\bar{P}}{dt} = -q$$

Combined productivity index equation:

$$J = \frac{q}{\bar{P} - P_{wf}} = J_\infty + \beta t^n$$

Rearrange the combined productivity index equation and insert into material balance equation for CRM

$$c_t V_p \frac{d\bar{P}}{dt} = -q = (J_\infty + \frac{\beta}{t^n})(\bar{P} - P_{wf})$$

$$c_t V_p \frac{d\bar{P}}{(\bar{P} - P_{wf})} = \left(J_\infty + \frac{\beta}{t^n}\right) dt$$

Integrate with respect to pressure difference and time respectively

$$c_t V_p \ln\left(\frac{\bar{P} - P_{wf}}{P_i - P_{wf}}\right) = -\left(Jt + \frac{\beta}{1-n} t^{1-n}\right)$$

$$\ln\left(\frac{\bar{P} - P_{wf}}{P_i - P_{wf}}\right) = -\left(\frac{t}{\tau} + \frac{\beta}{(1-n)ctV_p} t^{1-n}\right)$$

$$\bar{P} - P_{wf} = P_i - P_{wf} e^{-\left(\frac{t}{\tau} + \frac{\beta}{(1-n)ctV_p} t^{1-n}\right)}$$

$$q = J_\infty (P_i - P_{wf}) \left(1 + \frac{\beta}{Jt^n}\right) e^{-\left(\frac{t}{\tau} + \frac{\beta}{(1-n)ctV_p} t^{1-n}\right)}$$

Appendix B: Derivations of Logistic CRM

Material balance equation for CRM:

$$V_p c_t \frac{d\bar{P}}{dt} = -q$$

Logistic productivity index equation:

$$\bar{P} - P_{wf} = \frac{L}{(C + Qq^{-B})^{\frac{1}{v}}}$$

Rearrange the logistic productivity index equation and insert into material balance equation for CRM.

$$c_t V_p \frac{d\bar{P}}{dt} = c_t V_p \frac{d}{dt}\left(P_{wf} + \frac{L}{(C + Qq^{-B})^{\frac{1}{v}}}\right) = -c_t V_p L \frac{\frac{d}{dt}(C + Qq^{-B})^{\frac{1}{v}}}{(C + Qq^{-B})^{\frac{2}{v}}}$$

$$= -c_t V_p L \frac{\frac{1}{v}(C + Qq^{-B})^{\frac{1}{v}-1}\frac{d}{dt}(C + Qq^{-B})}{(C + Qq^{-B})^{\frac{2}{v}}} = -c_t V_p L \frac{\frac{1}{v}(C + Qq^{-B})^{\frac{1}{v}-1} Q \frac{d}{dt}(q^{-B})}{(C + Qq^{-B})^{\frac{2}{v}}}$$

$$= -\frac{c_t V_p LQ}{v} \frac{(C + Qq^{-B})^{\frac{1}{v}-1}(-Bq^{-B-1})\frac{dq}{dt}}{(C + Qq^{-B})^{\frac{2}{v}}} = -\frac{c_t V_p LQ}{v}(C + Qq^{-B})^{\frac{-v^2-1}{v}} q^{-B-1}\frac{dq}{dt}$$

$$\frac{dq}{dt} = -q^{B+2}(C + Qq^{-B})^{\frac{v^2+1}{v}} \frac{v}{c_t V_p LQB}$$

Because of the complexity of the equation, solve the above equation by explicit finite differences

$$\frac{q_{n+1} - q_n}{\Delta t} = -q_n^{B+2}(C + Qq_n^{-B})^{\frac{v^2+1}{v}} \frac{v}{c_t V_p LQB}$$

$$q_{n+1} = -q_n^{B+2}(C + Qq_n^{-B})^{\frac{v^2+1}{v}} \frac{v\Delta t}{c_t V_p LQB} + q_n$$

References

Albertoni, A., and Lake, L. W. 2003. *Inferring Connectivity Only From Well-Rate Fluctuations in Waterfloods*. SPEREE **6**(1):6-16

Albertoni, A. 2002. *Inferring Interwell Connectivity Only From Well-Rate Fluctuations in Waterfloods*. M.S. Thesis, The University of Texas at Austin

Bruce, W. A. 1943. *An Electrical Device for Analyzing Oil-Reservoir Behavior*. Trans. AIME **151**(1):112-124

Cao, F. 2014. *Development of a Two-Phase Flow Coupled Capacitance Resistance Model*. Ph.D. Dissertation, The University of Texas at Austin, Austin, Texas

Clark, J. C. *Decline Curve Analysis in Unconventional Resource Plays Using Logistic Growth Models*. M.S. Thesis. The University of Texas at Austin, Austin, Texas

El-Banbi, A. H. 1998. *Analysis of Tight Gas Well Performance*. Ph.D. Dissertation, Texas A&M University, College Station, Texas

Malthus, T. T. 1872. *An essay on the principle of population: or, A view of its past and present effects on human happiness; with an inquiry into our prospects respecting the future removal or mitigation of the evils which it occasions*. Reeves and Turner

Patzek, T. W. and Croft, G. D. 2010. *A Global Coal Production Forecast with Multi-Multi-Hubbert Cycle Analysis.* Energy **35**(8):3109-3122

Sayarpour, M. 2008. *Development and Application of Capacitance-Resistive Models to Water/CO_2 Floods.* Ph.D. Dissertation, The University of Texas at Austin, Austin, Texas

Tsoularis, A. and Wallace, J. 2001. *Analysis of Logistic Growth Models*. Mathematical Biosciences **179**(1):21-55

Verhulst, P. F., 1838. *Notice sur la loi que la population poursuit dans son accroissement*. Correspondance Mathematique et physique v.10

Wattenbarger, R. A., El-Banbi, A. H., Villegas, and M.E, Maggard, J.B. 1998. *Production Analysis of Linear Flow into Fractured Tight Gas Wells*. Paper SPE 39931, presented at the SPE Rocky Mountain Region/Low-Permeability Reservoirs Symposium and Exhibition, Denver, CO, Apr., 5-8

Walsh, M.P, and Lake, L.W. 2003. *A Generalized Approach to Primary Hydrocarbon Recovery of Petroleum Exploration & Production, Volume 4 (Handbook of Petroleum Exploration and Production)*, Elsevier Science.

Weber, D.B., Edgar, T.F., Lake, L.W., Lasdon, L.S., Kawas, S., and Sayarpour, M. 2009. *Improvements in Capacitance-Resistive Modeling and Optimization of Large Scale Reservoirs*. Paper SPE 121299, presented at the SPE Western Regional Meeting, San Jose, CA, Mar., 24-26

Weber, D.B. 2009. *The Use of Capacitance-Resistance Models to Optimize Injection Allocation and Well Location in Water Floods,* Ph.D. Dissertation, The University of Texas at Austin, Austin, Texas

Yousef, A. A., Gentil, P.H., Jensen, J.L., and Lake, L.W. 2006. *A Capacitance Model to Infer Interwell Connectivity from Production and Injection Rate Fluctuations*. SPEREE **9**(5):630-646

Yousef, A. A. 2005. *Investigating Statistical Techniques to Infer Interwell Connectivity from Production and Injection Rate Fluctuations*. Ph.D. Dissertation, The University of Texas at Austin, Austin, Texas